



Removal of phenol from aqueous solutions using adsorbents derived from low-cost agro-residues

Jhilly Dasgupta^a, Anuj Kumar^a, Dalia Dasgupta Mandal^b, Tamal Mandal^{a,*}, Siddhartha Datta^c

^aDepartment of Chemical Engineering, National Institute of Technology, Durgapur, West Bengal 713209, India, emails: jhillydasgupta@gmail.com (J. Dasgupta), anujibt@gmail.com (A. Kumar), Tel. +91 9434788078; emails: tamal_mandal@yahoo.com, prof.tamalmandal@gmail.com (T. Mandal)

^bDepartment of Biotechnology, National Institute of Technology, Durgapur, West Bengal 713209, India, Tel. +91 9434788141; email: daliadasguptamandal@gmail.com

^cDepartment of Chemical Engineering, Jadavpur University, Raja S.C. Mallik Road, Kolkata 700032, India, Tel. +91 33 2335 9345; Fax: +91 33 2413 7121; email: sdatta_che@rediffmail.com

Received 4 March 2015; Accepted 3 June 2015

ABSTRACT

Adsorption of phenol from its aqueous solutions using activated carbon, prepared from tomato stem, in a batch process was investigated. The preparation of charred tomato stem (CTS) activated carbon involved carbonization of the precursor previously impregnated with ortho-phosphoric acid activating agent (activating agent volume (ml) by precursor weight (g) ratio set at 1:1) at 470°C for 2 h. Equilibrium and kinetic studies were carried out using phenol solutions of various concentrations (20–100 mg/L). The adsorbent was characterized via electron probe microanalysis (EPMA) associated with energy dispersive spectrometry (EDS), Fourier transform Infrared analysis, pore volume and BET surface area determinations. Parametric study of the adsorption process was also conducted. The equilibrium adsorption data were elucidated using Langmuir, Freundlich, Dubinin–Radushkevich and Temkin isotherm models. Equilibrium data fitted satisfactorily to the Langmuir model; the maximum adsorption capacity was 41.6667 mg/g at 308 K. Pseudo-first-order and pseudo-second-order models suitably validated the adsorption kinetics while the intraparticle diffusion model and Boyd kinetic model examined the diffusion mechanism involved therein. Desorption studies were conducted using water, absolute ethanol (100% v/v) and 0.1 (N) NaOH solution as desorbing agents. Thermogravimetric analysis examined the thermal stability and regeneration potential of the CTS activated carbon.

Keywords: Activated carbon; Adsorbent; Isotherm models; Equilibrium; Kinetics

1. Introduction

Phenol is typically produced in the petrochemical, chemical and pharmaceutical industries, and is widely

used in the manufacture of resins for automobile industries, adhesives production and various other applications. Presence of phenolic compounds even at low concentration in the industrial wastewater adversely affects aquatic as well as human life directly

*Corresponding author.

or indirectly when disposed off to public sewage, river or surface water. Phenols are carcinogenic, mutagenic and teratogenic, and have been classified as priority pollutants by USEPA, which has thereby prescribed a permissible limit, lower than 1 mg/L, with regard to phenol discharge into the wastewater [1]. The concentration level of phenols in the industrial effluents for safe discharge into surface waters has been set at a maximum of 1.0 mg/L by the Ministry of Environment and Forests (MOEF), while the permissible concentration for phenols in potable waters recommended by WHO is 0.001 mg/L [2].

The conventional processes for removing phenolic compounds include techniques such as, oxidation with ozone in the presence of Fenton reagent [3], ion-exchange [4], electrocoagulation [5], biodegradation [6] and adsorption [7]. The treatment of phenol contaminated wastewater using adsorption has gained popularity as an effective method that overcomes many of the technical constraints suffered by other techniques, such as the large amount of chemicals used for oxidation processes, ion-exchange, etc. which become sources of secondary pollution, or the sensitivity of the biological treatment processes towards diurnal fluctuation and toxicity of some chemicals which is disadvantageous [8].

Adsorption using commercial activated carbon provides various advantages such as high porosity and excellent adsorption capacity due to its high surface area of the activated carbon surface. But the major constraints in the application of activated carbon include its high cost due to relatively expensive precursors (wood or coal), expensive regeneration and high regeneration loss, among others [8]; these handicaps can be overcome through application of alternative low-cost adsorbents prepared from various non-conventional waste materials obtained from industries and agriculture. Survey of literature however, reveals a dearth of quality research documented on the removal of the highly persistent phenol using activated carbon derived from agro-residues. Some of the recent attempts made to examine the removal of phenol using agricultural waste-based carbon include scientific investigations dealing with removal of phenol or its derivatives from aqueous solutions using activated carbon produced from avocado kernel seeds [9] and rice husk [10], analysis of adsorption of 2,4,6-trichlorophenol on oil palm empty fruit bunch-based activated carbon [11], development of effective technology for utilizing porous carbon from vinegar lees for phenol adsorption [12], study of phenol adsorption onto activated carbon derived from macadamia nut shells [13], etc.

Tomato stems have been chosen as raw materials for activated carbon production in the present study, owing to the growing popularity of tomato over the years as an important vegetable crop giving high yield, according to the survey conducted by National Horticulture Board [14]. However, utilization of tomato stems as raw materials to prepare activated carbon adsorbent has not been considered till date. In the present investigation, considerable effort has been made to valorize the tomato stems for the production of activated carbon after the harvest of tomatoes; this can significantly contribute to a healthier environment through sorption of pollutants like phenol, besides providing a feasible solution to the problem of disposal of the low-cost agro-residue and economizing the production and regeneration of adsorbents through the use of locally available cheap raw material. An attempt has also been made to apply thermogravimetric analysis (TGA) to determine the regeneration potential of charred tomato stem (CTS) activated carbons loaded with phenol by means of detailed scrutiny of the thermal stability results obtained from TGA plots, thus departing from the conventional techniques adopted in other reported investigations to study desorption of adsorbate from adsorbent [9,11].

2. Materials and methods

2.1. Adsorbate and solution

The adsorbate used here was analytical reagent grade phenol supplied by Merck, Mumbai, India. A stock solution of phenol was obtained by dissolving the required amount of phenol in distilled water and no pH adjustment was made. Working solutions of phenol having the desired concentrations were then prepared from the stock solution by successive dilutions.

2.2. Preparation of activated carbon

The tomato stems were collected from the local fields of Durgapur, just after the harvest of tomatoes. The stems were then washed with water to remove dust particles and were dried in sunlight for 2–3 d. Dried tomato stems were cut into small pieces, each piece about 2–3 cm in size and were ground using a mixer and grinder. The ground precursor was then sieved and particles having the size <90 μm were assorted. The activating agent used here is orthophosphoric acid (85% Pure, Merck, Mumbai, India), and the precursor was impregnated with requisite

amount of the activating agent in the (volume of acid, ml/weight of precursor, g) ratio of 1:1 and was then well mixed. This was then carbonized in a muffle furnace by heating at an elevated temperature of 470°C for 2 h. It is worth mentioning in this regard that the optimum time, temperature and impregnation ratio for carbonization had been estimated a priori with the help of response surface methodology (RSM), provided by Design Expert software 8.0.6; statistically designed experiments prescribed by a standard RSM design called central composite design (CCD) had thus been employed, and the optimization procedure had been carried out in accordance with process reported in literature [15]. The charred material was cooled and washed firstly with dilute ammonia solution (A.R. Grade, SARA Fine Chemicals Pvt. Limited) in order to get rid of any unconverted activating agent from carbonaceous material and then was washed continuously with distilled water until the pH of the filtrate was found to be exactly 7. The charred material left on the filter paper was then placed on a Petri dish and was left to dry overnight in an ambient condition. The dried samples were crushed and fractionated into different size fractions (in the present study the particles obtained were mostly in the size range of <90 µm) and CTS activated carbon was obtained.

2.3. Characterization of CTS activated carbon

Important physicochemical properties determined in the present investigation by means of standard procedures, with a view to characterize the CTS activated carbon prepared, comprise bulk density, ash content, volatile matter content, moisture content and fixed carbon content of CTS activated carbon. Surface area of CTS was determined by utilizing modified BET method for single-point surface area determination along with total pore volume using Bet surface area analyzer (Smart Instruments Company Private Limited, Mumbai, India). In all of these experiments, particles having the size < 90 µm were used to retain consistency in the results obtained.

2.3.1. Electron probe microanalysis (EPMA) associated with energy dispersive spectrometry (EDS)

The surface morphology of the prepared CTS activated carbon samples before and after phenol adsorption were examined by means of secondary electron imaging mode of EPMA (JXA-8230, JEOL) under an acceleration voltage of 15 kV and at a working distance of 25 mm. This SE image detector functions according to the principles adopted in

scanning electron microscopy; the topographic information about the samples was hence obtained. For preparing phenol-loaded activated carbon, 0.1 g of CTS activated carbon was contacted with 100 ml of 2,000 mg/L of aqueous phenol solution at 36°C for 24 h, in order to ensure 90–100% surface coverage by phenol. Elemental mapping was conducted on the activated carbon surface to detect the degree of incorporation of phosphorous into the CTS activated carbon impregnated with ortho-phosphoric acid activating agent. An elaborate distribution profile of phosphorous and other elemental constituents of activated carbon was obtained using an EDS appended to the electron probe microanalyser.

2.3.2. FTIR analysis

The functional groups present on the surface of the CTS activated carbon before and after phenol adsorption were detected by means of KBr technique using a Fourier transform infrared (FTIR) spectroscope (Perkin Elmer Model Spectrum RX1). The spectra were recorded in the 4,000–400 cm⁻¹ range.

2.4. Batch equilibrium, kinetic studies and effect of initial pH

2.4.1. Kinetic study

The objective of kinetic study is to elucidate the mechanism of adsorbate uptake by the adsorbent in question and also to evaluate the kinetic parameters that are critical to the designing of a continuous contactor. The information provided by thermodynamic data pertains only to the final state of the system, whereas kinetic study deals with the elucidation of the changes observed in the chemical properties of the system with time. The initial concentration of the adsorbate solution and the adsorbent dosage were varied in the following manner. It is worth mentioning that the size of the adsorbent, also a parameter, was omitted in this case as considerable amounts of the adsorbent were obtained mostly in the size range of <90 µm, and a negligible quantity exhibited sizes around 150 µm. The kinetic experiments were conducted in a set of 250-ml Erlenmeyer flasks, where solutions of phenol 100 ml each with different initial concentrations (20–100 mg/L) were added in these flasks. Equal quantities of 3 g/L of CTS of particle size <90 µm were added to the phenol solution in each of the flasks and the flasks were kept in an isothermal shaker of 150 rpm at 35 ± 1°C. Similarly, another set of Erlenmeyer flasks containing the same phenol concentration without activated carbon was used as a blank. The

unbuffered natural pH of each solution was 6.9. The aqueous samples were taken at preset time intervals that is at 20, 60, 120, 240, 1,380 and 1,440 min and the concentrations of phenol were measured by filtering the samples using Whatman No: 40 (W. & R. Balston, Ltd.) filter paper. The concentration of phenol in the filtrate was analysed using a double-beam UV–visible spectrophotometer (UV 2300, Techcom, Germany) at 270 nm wavelength [11,15].

In another similar experiment, the initial concentration of each solution was kept constant at 30 mg/L, while the adsorbent loading was varied as 1, 2, 3, 4 and 5 g/L, respectively, to study the effect of adsorbent dosage on the removal of phenol. The size of the adsorbent and pH of the solution were same as those in the previous set of experiments [15].

2.4.2. Equilibrium study

In the equilibrium study, experiments were conducted in a set of 250-ml Erlenmeyer flasks, where solutions of phenol 100 ml each with different initial concentrations (20–100 mg/L) were added in these flasks. Equal quantities of 3 g/L of CTS of particle size <90 μm were added to the phenol solution in each of the flasks and the flasks were kept in an isothermal shaker of 150 rpm at $35 \pm 1^\circ\text{C}$. Similarly, another set of Erlenmeyer flasks containing the same phenol concentration without activated carbon was used as a blank. The unbuffered natural pH of each solution was 6.9. The samples were equilibrated for 24 h, and thereafter the samples were filtered and the filtrates were spectrophotometrically analysed at 270 nm. The amount of adsorption at equilibrium, q_e (mg/g), was calculated by [11]:

$$q_e = \frac{(C_0 - C_e)V}{m} \quad (1)$$

where C_0 and C_e (mg/L) are the initial and equilibrium liquid-phase concentrations of phenol, respectively. V (L) is the volume of the adsorbate solution and m (g) is the mass of dry adsorbent used. The entire experiment was carried out separately at two different temperatures, 35°C (308 K) and 37°C (310 K), whereby the sensitivity of the current adsorption process to minor fluctuations in temperature, or, in other words, the variations in adsorption uptake of phenol and the trajectories traced by adsorption equilibrium following relatively modest fluctuations in the temperature of the problem milieu could be meticulously gauged and monitored [11].

2.4.3. Effect of initial pH

The effect of initial pH of the solution on the adsorption of phenol from its aqueous solution using CTS was studied in the pH range 2–11 at 35°C using 100 ml phenol solutions each having the initial phenol concentration of 30 mg/L, adsorbent dose of 3 g/L and a constant speed of agitation fixed at 150 rpm. The pH of the phenol solutions were adjusted as desired using a few drops of dilute N/10 NaOH and N/10 HCl. The contact time was varied from 20 min to 24 h. The pH was then measured [11].

2.5. Desorption studies

In the present study, the efficiency of each of the desorbing agents, namely water, absolute ethanol (100% v/v) and 0.1 (N) NaOH solution, in bringing about the desorption of adsorbed phenol from the surface of spent CTS activated carbon, was investigated. These desorbing agents were selected based on earlier studies reported in literature [13].

The phenol-loaded activated carbon sample was obtained by contacting 0.1 g of activated carbon with 100 ml of 2,000 mg/L of aqueous phenol solution, in accordance with the popular observation by Magne and Walker [16], that the concentration thus chosen corresponded to a surface coverage of 90–100% by phenol, owing to 0.522 nm^2 of surface area occupation by a single phenol molecule. The suspension was then shaken at 36°C for 24 h at an unbuffered pH of 6.05 in an isothermal shaker, with rotation speed of 150 rpm, and filtered thereafter. The fall in the concentration of phenol in the supernatant liquid, and hence the phenol uptake C_{ad} (mg/g of adsorbent) by the given weight of the adsorbent, was monitored using a double-beam UV–visible spectrophotometer (UV 2300, Techcom, Germany) at 270 nm wavelength. This was considered as the adsorption test. The entire experiment was performed in triplicates in order to obtain three separate activated carbon samples (each 0.1 g) loaded with phenol.

Each spent activated carbon separated from the solution after the adsorption test was then washed with deionized water to remove any unadsorbed phenol. Thereafter, these samples were dried at 110°C in an oven (Digitech System, Kolkata) and then added into separate Erlenmeyer flasks containing 100 ml of water, absolute ethanol (100% v/v) and 0.1(N) NaOH solution, respectively, for desorption of the phenol. The flasks were kept in the isothermal water bath shaker at the same temperature and for the same time duration as the adsorption tests. After desorption, the concentration of phenol desorbed in each case, C_{de}

(mg/g of adsorbent) from the given weight of the adsorbent was similarly measured using the UV–visible spectrophotometer. The percentage desorption is calculated as [11]:

$$\text{Desorption (\%)} = \frac{C_{\text{de}}}{C_{\text{ad}}} \times 100 \quad (2)$$

2.5.1. Application of TGA to examine regeneration potential of CTS activated carbon

Equal weights (0.1 g) of three samples, namely pristine CTS activated carbon sample, activated carbon sample loaded with phenol and spent activated carbon after treatment with absolute ethanol (100% v/v) desorbing agent, were separately subjected to programmed thermodesorption up to 850°C (1,123 K) after air-drying each sample at 110°C in an oven (Digitech System, Kolkata). Phenol-loaded activated carbon sample was obtained by subjecting a fresh CTS activated carbon sample (0.1 g) to similar adsorption test as followed during desorption studies. The ethanol-regenerated CTS activated carbon was obtained by means of the procedure undertaken while examining phenol desorption from CTS activated carbon. TGA was carried out using a Shimadzu Analyser, under 200 ml/min flow rate of pure nitrogen and a heating rate of 40°C/min, giving rise to a TGA curve characteristic of the sample under scrutiny [16].

3. Results and discussion

3.1. Characterization of CTS activated carbon

The resulting values of the different physicochemical properties of CTS activated carbon are listed in Table 1.

Table 1

Comparison between CTS activated carbon and commercial activated carbon in terms of different physicochemical properties

Properties	CTS activated carbon	Commercial activated carbon (approximate)	Ref.
Moisture content (wt %)	10.39	Variable (decreases with increase in temperature) Typically ≥ 4	[17]
Ash content (wt %)	5.77	5–6	[17]
Volatile matter content (wt %)	12.14	Variable (depends on raw material & history of carbonization)	[18]
Fixed carbon content (wt %)	71.70	Variable (depends on raw material & history of carbonization) Usually can be as low as <50 or as high as ~95	[17,18]
BET surface area (m ² /g)	850	800–1,500	[18]
Pore volume (cm ³ /g)	0.5904	0.20–0.60	[18]
Bulk density (g/cm ³)	0.36	0.25–0.75	[19]

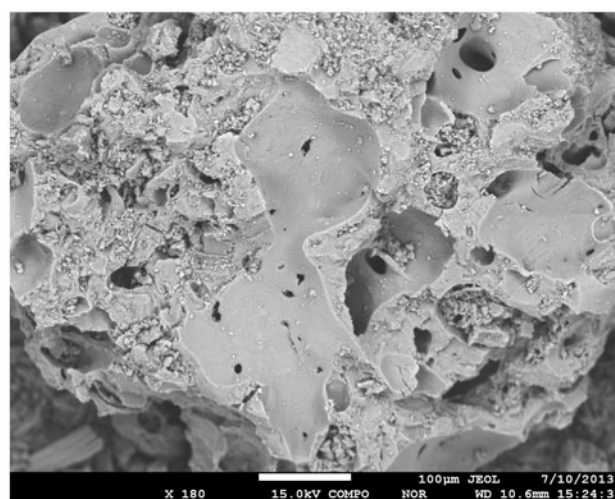
Bulk density of activated carbon is defined as the mass of a unit volume of the sample in air, and this includes both the pore system and the voids among the particles. It is very useful in estimating the packing volume or in evaluating the grade of carbon needed for an existing system. The raw material, the particle size used and the degree of activation have a significant influence on the bulk density, which in turn suitably monitors the adsorption per unit volume [17]. Specific surface area of an adsorbent is indicative of the adsorbent efficiency in terms of extent of adsorption uptake, which, for particles of suitable molecular size, increases with an increase in specific surface area. However, the size of the particles that can be adsorbed is delimited by the pore volume. The pore volume obtained in the present case was 0.5904 cm³/g; the recorded pore volume was comparable to that of high-quality commercial activated carbon that has a pore volume in the range 0.2–0.6 cm³/g [18] as exhibited in Table 1. The adsorption process is influenced by the mineral matter content of the carbon derived from the source materials and from activating agents added during manufacture. Hence, the total amount of inorganic constituents will vary from one grade of carbon to another. High mineral matter content has a deleterious effect on the adsorption performance of activated carbon because it tends to block the porosity of the carbon matrix and can preferentially adsorb water because of its hydrophilic nature, hence increasing the hydrophilicity of activated carbon while reducing the adsorption of the adsorbate [19]. Owing to the catalytic effects of the inorganic mineral matter content, restructuring of the adsorbent during regeneration of used activated carbon might also be witnessed. This inorganic material contained in activated carbon is measured as ash content which can be

defined as the residue that remains when the carbonaceous materials is burned off. In general, ash content of activated carbons is around 5–6% [17]. A small increase in ash content is detrimental to the adsorptive properties of activated carbons. Besides, it reduces the mechanical strength of carbon. The presence of ash has been shown to inhibit surface development. The moisture content does not have much effect on the adsorptive power, but obviously it dilutes the carbon [19]. This necessitates an additional weight of moist carbon to provide the required dry weight. A good quality activated carbon, therefore, should have low ash and moisture content and high fixed carbon content. The comparison made between CTS activated carbon and commercial activated carbon in terms of the parameters discussed above clearly qualifies the CTS activated carbon under study as a competitive candidate, with regard to both cost and quality, for application as a satisfactory replacement of the relatively expensive commercial activated carbon.

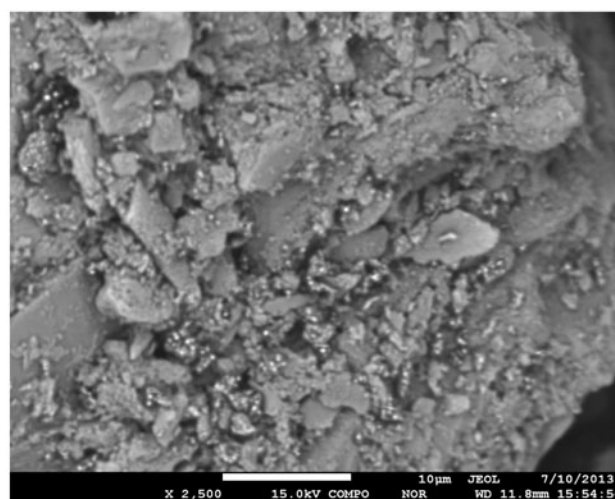
3.2. Electron probe microanalysis (EPMA) associated with energy dispersive spectrometry (EDS)

The EPMA generated secondary electron (SE) images of CTS activated carbon before and after phenol adsorption are exhibited in Fig. 1(a) and (b), respectively.

Fig. 1(a) demonstrated the heterogeneous topography of CTS activated carbon surface, where the small crater like micropores could be identified. Besides, the presence of randomly distributed larger pores of different sizes, as shown in Fig. 1(a), suggested the development of mesoporosity and macroporosity along with microporosity during the process of formation of activated carbon. The cellular structure of the original biomass was also visualized in the figures. Moreover, the unevenly distributed bright spots on the carbon surface, as revealed in the SE images, indicated the presence of ash contents in the carbon grains [20]. These observations can be explained with reasonable accuracy with the help surface development mechanism of activated carbon during the carbonization and activation process. According to findings of Bansal and Goyal [18], during the carbonization process, most of the non-carbon elements such as oxygen, hydrogen and nitrogen are driven off as volatile gaseous species by the pyrolytic decomposition of the precursor. The residual elementary carbon atoms group themselves into stacks of flat, aromatic sheets cross-linked in a random manner. These aromatic sheets are irregularly arranged, which leaves free interstices. These interstices give rise to pores, which make activated carbons excellent adsorbents.



(a)



(b)

Fig. 1. SE image of (a) CTS activated carbon (scale bar is 100 μm) and (b) CTS activated carbon loaded with phenol prepared by contacting 0.1 g of CTS activated carbon with 100 ml of 2,000 mg/L of aqueous phenol solution at 36°C for 24 h, (scale bar is 10 μm).

Activated carbons have a microcrystalline structure. But this microcrystalline structure differs from that of graphite with respect to interlayer spacing, which is 0.335 nm in the case of graphite and ranges between 0.34 and 0.35 nm in activated carbons. The orientation of the stacks of aromatic sheets is also different, being less ordered in activated carbons. The term *turbostratic* was proposed by Biscoe and Warren to describe the structure, the disorder in the microcrystallite layers being mainly due to the presence of heteroatoms such as hydrogen and oxygen, and by defects such as vacant lattice sites in the structure of activated carbons [18]. Activated carbon is thus an assembly of defective

graphene layers. During carbonization, these pores get filled with the tarry matter or the products of decomposition or at least blocked partially by disorganized carbon. This pore structure is further enhanced through activation process which clears off the spaces between the aromatic sheets are of various carbonaceous compounds and disorganized carbon [18]. The decisive role played by ortho-phosphoric acid to precursor is worth mentioning. Earlier studies reveal that there is a rapid development of microporosity from low concentrations of ortho-phosphoric acid. The degree of activation is indicated by the amount of phosphorous that is incorporated into the particles, X_p , which ranges from 0.09 to 0.91 g (P)/g precursor [21]. Microporosity is the predominant porosity up to $X_p = 0.3$, with pore volumes reaching up to $0.6 \text{ cm}^3/\text{g}$. With further increase in concentrations of H_3PO_4 , the development of microporosity is negligible, development of mesoporosity is predominant, and it reaches values higher than the micropore volume. A relatively smoother activated carbon surface was visualized in the SE image for phenol-loaded CTS activated carbon exhibited in Fig. 1(b). This observation can be attributed to the filling of the pores present on the carbon surface by the adsorbed phenol, thus implying that the well-developed porous structure and the resulting extended surface area of the activated carbon are critical factors governing its adsorption capacity [22].

The preparation of activated carbon by carbonization and chemical activation of lignocellulosic materials such as biomass derived from agricultural wastes using phosphoric acid as activating agent, in many instances, might involve higher impregnation ratios, as reported in literature [23]. The impregnation ratio employed in the present study is 1.45 g/g, thus justifying the contribution of phosphoric acid to the development of heterogeneous porous structure on the CTS activated carbon surface with the carbonized raw material converted into a form that contains the greatest possible number of randomly distributed pores of various sizes and shapes, which gives rise to an extended and extremely high surface area of the product [18]. The commendable contribution of phosphoric acid to the development of heterogeneous well-developed porous morphology of CTS activated carbon accompanied with considerably high carbon yield (Table 1) hence warranted its success as an activating agent.

Particles impregnated with phosphoric acid develop a certain degree of elasticity which is explained as follows. The acid separates the cellulose fibres producing a partial de-polymerization of hemicellulose and lignin (the main components of the matrix). This causes a decrease in mechanical resistance. The factors mentioned above result in swelling

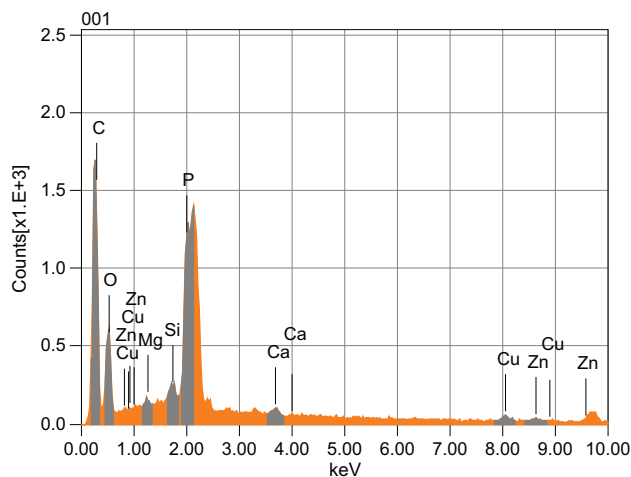


Fig. 2. Energy dispersive spectrometric (EDS) spectra of CTS activated carbon.

of the particle. Impregnation with ortho-phosphoric acid also sets off the conversion of the precursor to activated carbon which is evident from a significant amount of tar is observed on the surface of the particles, which may have been caused due to the de-polymerization of cellulose when catalyzed by phosphoric acid. This is then followed by dehydration and condensation (these reactions are also catalyzed by the acid), inducing the formation of more aromatic and reactive products, accompanied by some cross-linking as was observed in other reported investigations [19]. The additional cross-linking may be caused by the presence of phosphates. The compositional analysis of CTS activated carbon sample was highlighted in the energy dispersive spectrometric (EDS) spectra presented in Fig. 2.

The figure displayed the elemental mapping of the activated carbon surface, where the incorporated phosphorous stood out as an abundant constituent of CTS activated carbon, albeit with localized distribution, besides elements C and O. The EDS spectra further corroborated the conclusion drawn earlier from characterization of CTS activated carbon, which had suggested that the activated carbon material being scrutinized was rich in carbon content. Other elements such as Mg, Si, Ca, Cu and Zn were randomly dispersed throughout the material, and these elements indicated the presence of inorganic mineral matter in activated carbon [20].

3.3. FTIR study

Infrared spectroscopy (IR) in its various forms has been immensely effective in providing useful and

authentic information about surface functional groups on carbons. The infrared spectrum of CTS activated carbon before adsorption is presented in Fig. 3(a) [upper spectrum] and that after adsorption is shown in Fig. 3(b) [lower spectrum].

The IR spectrum of CTS, as shown in these figures, gives us an insight into the adsorption behaviour of CTS and the kind of interaction taking place between the activated carbon adsorbent and the phenol that is being adsorbed on to CTS activated carbon, as is indicated by the frequency changes in the functional groups of the activated carbon adsorbent and hence shifting of peaks in the IR spectrum of CTS after phenol adsorption. Fig. 3(a) reveals broad band at $3,400.45\text{ cm}^{-1}$ corresponding to the stretch vibration of hydrogen-bonded hydroxyl groups on the surface of CTS activated carbon [15]; the significant broadening of the absorption band and lowering of the mean absorption frequency suggested extensive hydrogen bond formation with other hydroxyl groups existing within the same molecule (intramolecular hydrogen bonding) or in neighbouring molecules (intermolecular hydrogen bonding). The lowering of the frequency is thus a function of the strength and degree of the hydrogen bonding [24]. The peak at $2,929.97\text{ cm}^{-1}$ could be attributed to the asymmetrical aliphatic (saturated) C–H stretch vibration ($-\text{CH}_3$ group). The aromatic ring stretch vibration was represented by a prominent peak at $1,596.86\text{ cm}^{-1}$, while the sharp absorption peak at $1,400.12\text{ cm}^{-1}$ accompanied by

weak overtone bands visualized as jagged craziness in the $2,000\text{--}1,650\text{ cm}^{-1}$ region indicated skeletal vibrations of aromatic ring (including C–C stretching within the ring) containing delocalized π electrons from the resonance-stabilized double bonds [25]. Careful examination of the absorption bands can give us a fair insight into the substitution pattern on an aromatic ring. The presence of two peaks at $1,578.14$ and $1,560.40\text{ cm}^{-1}$, respectively, corresponded to asymmetric stretching vibration of the NO_2 group while the broad band at $1,263\text{ cm}^{-1}$ was assigned to the overlap between symmetric stretch vibration of the NO_2 group and primary or secondary, OH in-plane bend [24,25]. The weak absorption band at $1,088.48\text{ cm}^{-1}$ suggested C–O stretching and O–H bending modes of alcoholic and phenolic groups [26]. The IR band at 670.09 cm^{-1} indicated $=\text{C}-\text{H}$ (“oop” bending) of aromatics; hence, fairly hinting at the presence of aromatic characters on the surface of CTS activated carbon. The medium band observed at 519.65 cm^{-1} represented the C–Br stretch of alkyl halides [24,25].

Detailed and careful examination of the shift or disappearance of peaks in IR spectrum of CTS activated carbon loaded with phenol exhibited in Fig. 3(b) revealed the nature of interaction taking place between the phenol and the activated carbon material. The disappearance of the peak at $1,400.12\text{ cm}^{-1}$ and shift in the peak at $1,596.86\text{--}1,586.98\text{ cm}^{-1}$ indicated that the adsorption was driven by the $\pi\text{--}\pi$ dispersion interactions between the aromatic ring of phenol and

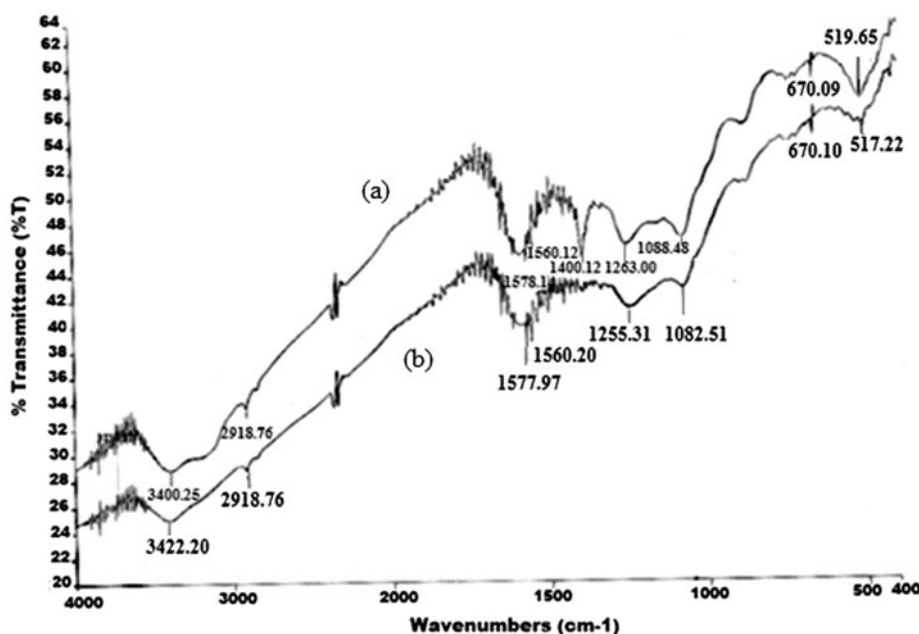


Fig. 3. Infrared spectrum of CTS activated carbon (a) before phenol adsorption (upper spectrum) and (b) after adsorption of phenol (lower spectrum).

the aromaticity of the graphene layers as was suggested by Coughlin and Ezra [27]. Besides, the phenolic groups present, being electron releasing groups, were probably responsible for the increase in the electronic density of the graphene layers, hence, affecting the dispersion interactions between the carbon surface and the molecules of the adsorbate [19]. The slight shift in the peaks present at 3,400.45 and 1,088.48 cm^{-1} to 3,422.20 and 1,082.51 cm^{-1} , respectively, could be attributed to the bonding of water molecules to the oxide functional groups by H-bonding; the water molecules, adsorbed on oxygen groups, subsequently, as secondary adsorption centres, retained other water molecules by means of H-bonds [19]. These resulting persistent complexes then blocked the entry of organic phenol molecules to significant parts of the activated carbon surface, thus reducing the phenol uptake. The peaks corresponding to the nitro groups were negligibly affected by phenol adsorption; this might have occurred owing to the electron withdrawing nature of the nitro groups which tend to remove electrons from the π -electron system, thus creating positive holes in the conducting π -band of the graphene layers. Consequently, the interactions between the π -electrons of the phenol aromatic ring and the π -electrons of the graphene layers were weak, thereby reducing the phenol uptake at these potentially active interaction sites [19,27]. No other significant change was observed in the other peaks present after phenol adsorption.

3.4. Parametric study of the adsorption process

3.4.1. Effect of contact time

Fig. 4(a) exhibits the effect of contact time and initial concentration of adsorbate solutions on the removal of phenol for different initial concentrations of phenol (20–100 mg/L) in terms of q_t , amount of phenol adsorbed per unit mass of adsorbent, as a function of time. The rate of adsorption was initially rapid and marked by a steep rise in the trajectory of the saturation curves. This observation indicated the presence of a large number of accessible vacant sites on the surface of the adsorbent. Eventually, the curves were found to level off to a plateau and the contact time corresponding to the attainment of dynamic equilibrium was 4 h at each concentration [19]. The leveling off implied that the vacant sites of the adsorbent were saturated at this level. About 60–70% of the adsorption capacity of CTS for phenol was achieved within 2 h, and thereafter adsorption rate declined. The decrease in the rate of phenol adsorption could also be attributed to the change in the adsorption mechanism, besides saturation of the active sites of

CTS activated carbon, following the development of chemisorption to the detriment of physisorption. The plateau attained was smooth indicating that unimolecular surface coverage has been achieved.

3.4.2. Effect of concentration

Spectacular escalation in the adsorption uptake was observed in Fig. 4(a) with an increase in initial concentration of the phenol solution. The equilibrium amount adsorbed per gram of adsorbent rose from 5.5 to 32.76 mg/g as the initial concentration of the phenol solution increased from 30 to 100 mg/L, owing to increase in driving force for mass transfer, that is, an increase in their difference between the bulk concentration of solute and the corresponding equilibrium solution concentration [28].

3.4.3. Effect of adsorbent dosage

Fig. 4(b) depicts the variation of adsorption uptake of phenol with variation in adsorbent dosage. It is obvious that the dramatic enhancement in the surface area available for adsorption due to increase in adsorbent loading was responsible for the resulting rise observed in the percentage removal of phenol [29]. As shown in Fig. 4(b), about 92% phenol removal was brought about in a 100 ml solution of 30 mg/L phenol solution with an adsorbent loading of 3 g/L. It was also observed that a further increase in the adsorbent dosage could achieve only a marginal increase in the percentage of phenol removed. Hence, it could be concluded that the optimum CTS adsorbent dosage for treating 30 mg/L phenol solution was 3 g/L.

3.4.4. Effect of initial pH

Effect of initial solution pH on the removal of phenol using CTS activated carbon can be suitably explained by means of three possible interactions reported by Bansal and Goyal [18], between the adsorbate (phenol, in this case) and the adsorbent, namely, (1) π - π dispersion interaction between the aromatic ring of the adsorbate and of the graphite structure, (2) electron donor-acceptor interaction between the aromatic ring and the basic surface sites and (3) electrostatic attraction and repulsion interaction.

The π - π dispersion effect was suggested by scientists Coughlin and Ezra [27], who essentially proposed one more mechanism, that is hydrogen bond formation, wherein, the water molecules bound to the oxide functional groups by H-bonding, in turn retained other water molecules as secondary adsorption sites,

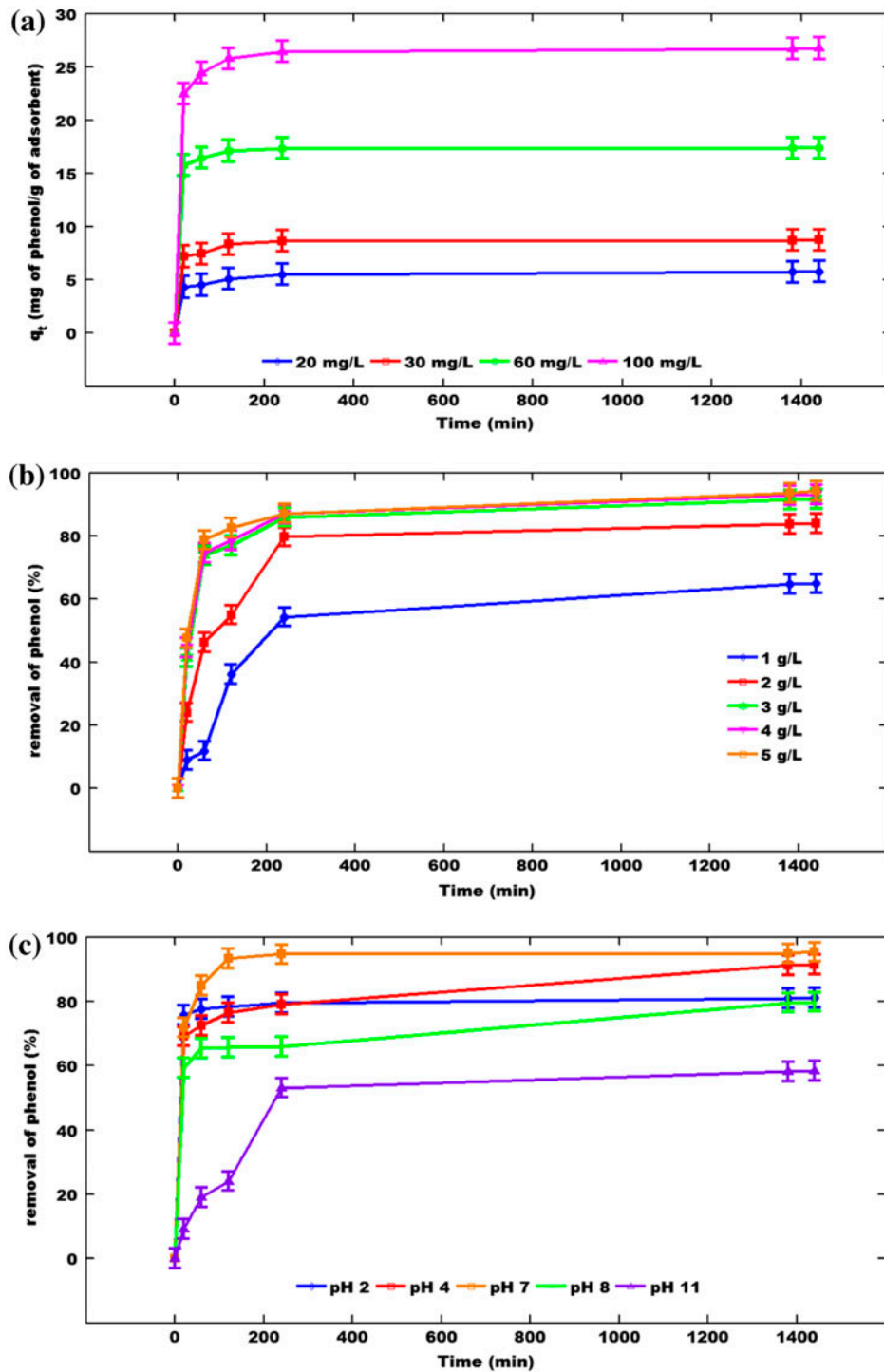


Fig. 4. (a) The variation of adsorption uptake with time at various initial phenol concentrations (adsorbent dosage: 3 g/L; pH 6.90; temperature: $35 \pm 1^\circ\text{C}$). (b) The variation of % phenol removal with time for different adsorbent dosage (initial concentration of phenol solution: 30 mg/L; pH 6.90; temperature: $35 \pm 1^\circ\text{C}$). (c) Effect of solution pH on adsorption of phenol onto CTS activated carbon (initial concentration of phenol solution: 30 mg/L; adsorbent dosage: 3 g/L; temperature: $35 \pm 1^\circ\text{C}$).

by means of H-bonds. These complexes then blocked the entry of the target phenol molecules to significant parts of the activated carbon surface. The electron donor–acceptor mechanism was suggested by Mattson et al. [30]. Additionally, electrostatic interactions also played an important role in controlling the adsorption process, particularly in adsorption of phenol which is a weak electrolyte. These interactions would in turn be governed by pH of the adsorbate solutions as well as acid–base character of the surface of the adsorbent.

Fig. 4(c) shows the effect of pH of the solution on the adsorption of phenol on the surface of CTS. Analysis of the results and trends of the graphs revealed that adsorption of phenol would increase gradually as the pH was varied from 2 to 7 and was highest at pH 7, beyond which a significant drop in the adsorption of phenol was witnessed. Hence, it could be concluded that pH 7 was the optimum pH for carrying out adsorption in the present investigation. This could be attributed to the fact that at lower acidic pH values of the adsorbate solution, the surface charges on the adsorbent were positive, on an average, that is, both the carbon–oxygen surface groups of CTS activated carbon and the adsorbate phenol were present in unionized form and as such, they were either positively charged or neutral. This resulted in weak dispersive interactions between the π electrons of the aromatic ring and the delocalized π electrons of the graphene layers of CTS. The pH of the solution also induces the dissociation or ionization of acidic electrolytes by means of controlling their pK_a . The ionic fraction of phenolate ion ϕ_{ions} can be estimated from the following correlation [31]:

$$\phi_{\text{ions}} = \frac{1}{[1 + 10^{(pK_a - \text{pH})}]} \quad (3)$$

The increase in pH of the solution causes ϕ_{ions} to increase. Phenol is a weak organic acidic compound with $pK_a \approx 9.89$ [29]. Hence, at basic pH values >7 , that is at $\text{pH} > pK_a$, the phenols dissociated to give phenolate ($\text{C}_6\text{H}_5\text{O}^-$) ions which were negatively charged. At such high basic pH values, the functional groups (acidic) at the surface of the adsorbent ionized as well, either partially or completely to give the surface of the adsorbent a negative charge. As a result, electrostatic repulsive interactions between the CTS surface and the phenolate ions and between the phenolate ions in solution, led to a decline in the uptake of the adsorbate, as is evident from the graphs. However, some dispersive interactions might have still occurred. Moreover, formation of electron donor–acceptor complexes could take place to a certain

extent, owing to the presence of some undissociated basic functional groups at the surface of the adsorbent. Thus, all the three forms of interactive forces in action, that determined the degree of adsorption that is taking place, were governed by the pH of the adsorbate solution [9,18].

3.5. Adsorption isotherms

Adsorption isotherm is the most extensively employed method used to represent the state of equilibrium of an adsorption system. Careful and detailed analysis of the evaluated parameters characterizing each isotherm reveals important surface properties of the adsorbent and helps in estimating the affinity of the specific adsorbent under investigation for the target pollutant, and the degree and mechanism of interaction between the adsorbent and adsorbate. Besides, they can also be used to make a comparison of the adsorptive capacities of the adsorbent for different pollutants. In the present study, the Langmuir, Freundlich, Temkin and Dubinin–Radushkevich isotherm models were used to describe the relationship between the equilibrium surface concentration (amount adsorbed per unit mass of adsorbent) and solution concentration of phenol. In this regard, it is worth mentioning that the plots in Fig. 4, showing the variations in adsorption uptake of phenol as a function of time, had revealed a fair attainment of dynamic equilibrium by the adsorbate–adsorbent system after about 300 min. Nevertheless, the equilibrium studies were conducted over a span of 24 h, so as to enable complete attainment of adsorbate–adsorbent equilibrium, in the face of inadvertent, erratic and at times imperceptible fluctuations in the problem environment or unpremeditated process instabilities encountered during the course of the experiment, which often tend to impede or disturb the state of equilibrium of the system [28,29].

The 4-h period required by the adsorbate–adsorbent to attain equilibrium can moreover be elucidated by the fact that the adsorption process investigated in the present study probably involved chemical sorption, wherein the adsorption of the solute phenol molecules onto the adsorbent surface was predominantly governed by weak dispersive interactions between the π electrons of the aromatic ring and the delocalized π electrons of the graphene layers of CTS adsorbent; in such cases, usually the solute molecules tend to escape from the adsorbent surface, following inadvertent fluctuations in the problem milieu. This phenomenon often entails prolonged contact times, as witnessed in the present case [18,27,28]. Nevertheless,

the time required by the present system to reach dynamic equilibrium is still adequately comparable with the observations reported in this regard by many of the adsorption based studies available in archival literature [11,29].

3.5.1. The Langmuir isotherm model

The Langmuir isotherm equation can be expressed as [29,32,33]:

$$q_e = \frac{q_{\max} b C_e}{1 + b C_e} \quad (4)$$

where C_e (mg/L) is the equilibrium solution concentration of the adsorbate, q_e (mg of adsorbate/g of adsorbent) is the equilibrium amount of adsorbate adsorbed per unit mass of adsorbent, while b and q_{\max} are Langmuir constants.

The linear form Langmuir isotherm equation is shown as follows:

$$\frac{C_e}{q_e} = \frac{1}{q_{\max} b} + \frac{C_e}{q_{\max}} \quad (5)$$

The constant q_{\max} is the surface concentration at monolayer coverage and represents the maximum value of q_e that can be obtained as C_e is increased. The constant b corresponds to the energy of adsorption and increases as the strength of the adsorption bond increases.

Fig. 5(a) exhibits a linear relationship of C_e/q_e vs. C_e using experimental data obtained, suggesting that the Langmuir model was applicable ($R^2 = 0.999$ and 0.965 for 308 and 310 K respectively). The main model postulates [18] are enumerated as: (1) the attachment of the adsorbed entities (atoms or molecules or ions) to the surface at definite localized sites; (2) incorporation of only a single adsorbed entity in each site; and (3) the assumption of a perfectly smooth and thermodynamically homogenous surface, where the energy state of each adsorbed entity is the same at all sites on the surface independent of the presence or absence of other adsorbed entities at neighbouring sites with negligible lateral interactions between the adsorbed entities. These propositions were adequately satisfied by the successful fitting of the experimental adsorption data using the Langmuir isotherm equation. The applicability of the model suggests that the mechanism followed during the adsorption of phenol onto CTS activated carbon thus conformed reasonably to the Langmuir isotherm model assumption of

monolayer coverage of the adsorbate at the outer surface of the adsorbent. Values of q_{\max} and b were calculated from the slope and intercept values of the plot shown in Fig. 5(a) and are listed in Table 2.

The adequacy of the Langmuir isotherm model was further justified by judicious examination of a dimensionless separation parameter (R_L), commonly known as separation factor and defined by Webber and Chakkravorti, as follows [26,34]:

$$R_L = \frac{1}{1 + b C_0} \quad (6)$$

The evaluated value of R_L determines whether the isotherm is unfavourable ($R_L > 1$), linear ($R_L = 1$), favourable ($0 < R_L < 1$) or irreversible ($R_L = 0$). The values of R_L shown in Table 2 indicated that the Langmuir isotherm model was favourable for representing the process of adsorption of phenol onto CTS activated carbon.

The value of b was found to increase only marginally and the value of q_{\max} was found to decrease with increase in temperature, thus suggesting that the adsorption of phenol onto CTS might be exothermic in nature and was favoured at a lowered temperature. A decrease in maximum adsorption uptake with increase in temperature was hence justified by the weakening of binding forces between the adsorbate and adsorbent with the corresponding increase in thermal energies of the sorbate [18]; similar observations were reported by Larous and Meniai [33], while investigating the adsorption of phenol onto sawdust. A comparison between the maximum monolayer phenol adsorption capacity of CTS activated carbon and some of other activated carbons available in the literature is shown in Table 3.

The value of q_{\max} obtained in the present study was found to be relatively higher than the values reported by other similar investigations, clearly hinting at the excellent phenol adsorption potential of CTS activated carbon.

3.5.2. Freundlich isotherm model

Freundlich isotherm model [34] is the earliest known empirical model describing the non-ideal and reversible adsorption. The Freundlich isotherm equation has the form

$$q_e = K_F C_e^{1/n} \quad (7)$$

which can be linearized as follows,

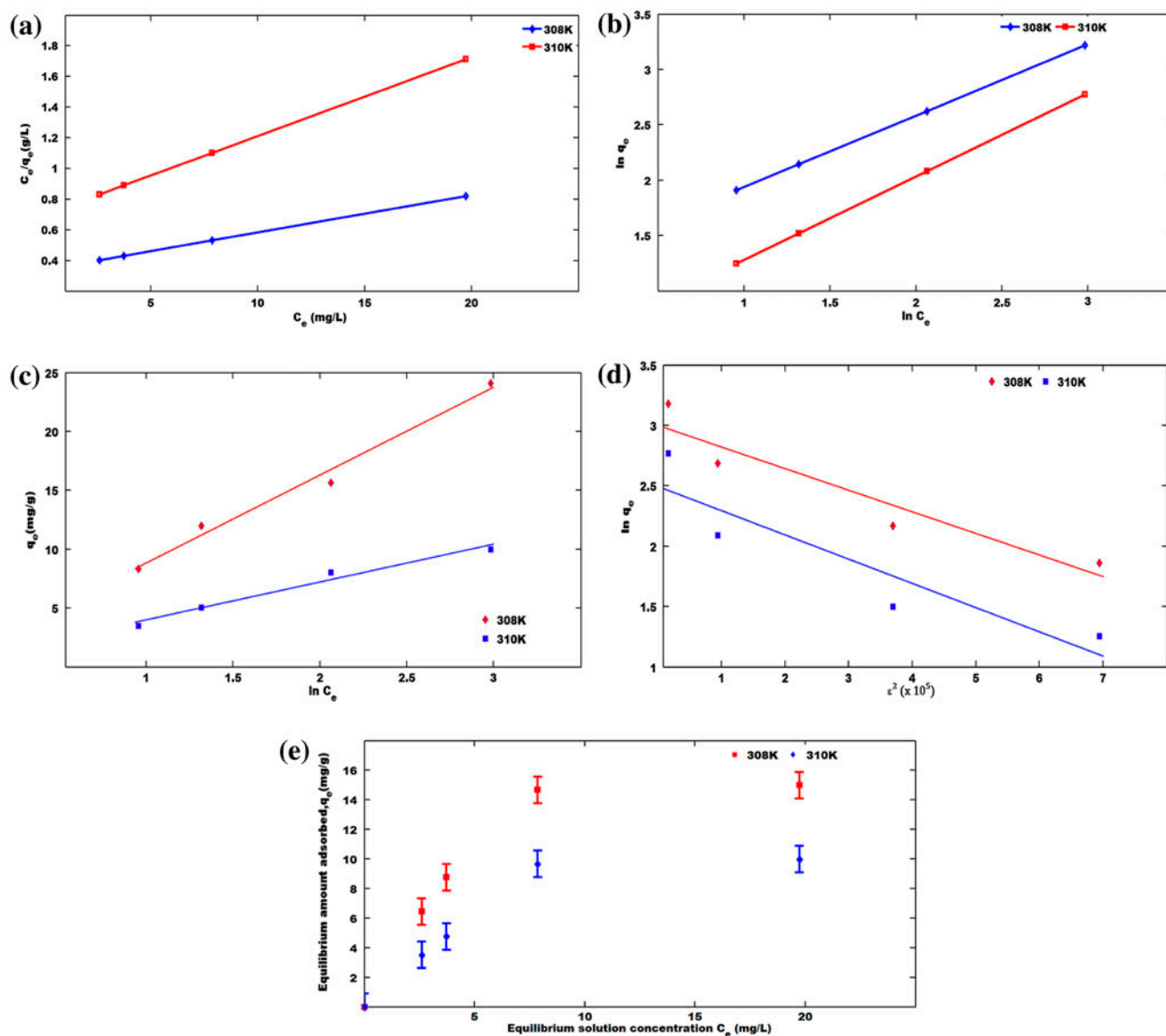


Fig. 5. (a) Langmuir adsorption isotherm for adsorption of phenol onto CTS activated carbon at temperatures 35°C (308 K) and 37°C (310 K). (b) Freundlich adsorption isotherm for adsorption of phenol onto CTS activated carbon at temperatures 35°C (308 K) and 37°C (310 K). (c) Temkin adsorption isotherm for adsorption of phenol onto CTS activated carbon at temperatures 35°C (308 K) and 37°C (310 K). (d) Dubinin–Radushkevich adsorption isotherm for adsorption of phenol onto CTS activated carbon at temperatures 35°C (308 K) and 37°C (310 K). (e) Type I adsorption isotherm for adsorption of phenol onto CTS at various temperatures.

$$\ln q_e = \ln K_F + (1/n) \ln C_e \quad (8)$$

The parameter K_F in the Freundlich equation is related mainly to the capacity of the adsorbent for the adsorbate and $1/n$ is a function of the strength of adsorption. When the values of C_e and $1/n$ are fixed, the larger the value of K_F , the larger is the capacity q_e . For fixed values of K_F and C_e , the decrease in the

value of $1/n$ leads to an increase in the strength of the adsorption bond. As $1/n$ becomes very small, the capacity for adsorption tends to be independent of C_e , resulting in irreversibility of the isotherm. If the value of $1/n$ is large, the adsorption bond becomes weak, and the value of q_e shows marked change for small changes in C_e [32]. The slope ranges between 0 and 1 and is a measure of adsorption intensity or surface heterogeneity; the surface heterogeneity increases as

Table 2
The parameters of Langmuir adsorption isotherm model

Concentration (mg/L)	Temperature (K)	R_L	b (L/mg)	q_{max} (mg/g)	R^2
20	308	0.413919	0.070796	41.66667	0.999
30		0.320113			
60		0.190556			
100		0.123768			
20	310	0.360676	0.088629	18.86792	0.965
30		0.273309			
60		0.158285			
100		0.10139			

Table 3
Comparison of the maximum monolayer phenol adsorption capacity on various low-cost adsorbents

Adsorbent	q_{max} (mg/g)	Ref.
Wood FA	5.4	[8]
Rice husk	4.508	[8]
AC from rubber seed coat	15.5	[8]
Sugarcane bagasse fly ash (BFA)	23.832	[35]
Activated carbon commercial grade (ACC)	30.2187	[35]
Laboratory grade activated carbon (ACL)	24.6458	[35]
Charred tomato stem (CTS) activated carbon	41.66667	Present study

the value of $1/n$ gets closer to zero. Thus, a value of $n > 1$ implies favourable adsorption process condition.

The plot of $\ln(q_e)$ against $\ln(C_e)$ is shown in Fig. 5(b). The value of n at either of the temperatures 308 and 310 K was found to be greater than 1, thereby indicating a favourable adsorption condition. The values of n and K_F at different temperatures are shown in Table 4.

The R^2 values observed at temperatures 308 and 310 K were 0.992 and 0.995, respectively, the values indicated that the Freundlich isotherm model satisfactorily represented the adsorption process. This empirical model can be successfully employed to define both monolayer and multilayer adsorption characterized by non-uniform distribution of heat of adsorption and affinity over thermodynamically heterogeneous surface; this unique model attribute thus accounted for the pertinence of Freundlich isotherm model in the representation of the same equilibrium adsorption data, which had earlier been fitted to Langmuir isotherm model (Fig. 5(a)). The surface heterogeneity previously ignored by the Langmuir isotherm, was taken into account as indicated by the values of n (>1) obtained. The validity of both the models in the concentration range under scrutiny was thus affirmed [29].

Table 4
Parameters of Freundlich isotherm, Temkin isotherm and Dubinin–Radushkevich isotherm

Parameters	308 K	310 K
Parameters of Freundlich isotherm		
n	1.550388	1.464129
K_F ((mg/g)(L/mg) ^{1/n})	3.647347	1.813031
R^2	0.992	0.995
Parameters of Temkin isotherm		
A (L/g)	1.200346	1.050443
B	7.464	3.678
b_T (J/mol)	343.075	700.744
R^2	0.984	0.974
Parameters of Dubinin–Radushkevich isotherm		
q_s (mg/g)	20.06546	7.901084
E (kJ/mol)	500	745.356
R^2	0.895	0.872

3.5.3. Temkin isotherm

Study of Temkin isotherm was carried out to examine the distribution of heat of adsorption and binding energy on the activated carbon surface. The

linear form of Temkin isotherm takes the following form [36]:

$$q_e = \left(\frac{RT}{b_T}\right) \ln A + \left(\frac{RT}{b_T}\right) \ln C_e \quad (9)$$

where $1/b_T$ represents the adsorption capacity or potential of the adsorbent and A is the Temkin isotherm constant; $\left(\frac{RT}{b_T}\right)$ can be taken as B . The Temkin isotherm model contains a factor that specifically takes into the account the adsorbent–adsorbate interactions. The plot of q_e vs. $\ln C_e$ is shown in Fig. 5(c). The constants A and B and correlation coefficient R^2 at temperatures 308 and 310 K are listed in Table 4.

The values of the correlation coefficient obtained were lower than those observed for the Langmuir and Freundlich isotherms, hence suggesting that the Temkin isotherm was relatively less suitable as compared to Langmuir and Freundlich isotherms for satisfactory representation of the equilibrium data in the present case. It can thus be concluded that the adsorption process did not adequately follow the assumptions of the Temkin isotherm, namely (1) a linear rather than a logarithmic decline in heat of adsorption (which is a function of temperature) of all molecules in the layer with surface coverage, which may occur due to repulsive forces on the uniform surface or due to surface heterogeneity of the adsorbent and (2) uniform distribution of binding energies of the adsorbent for the target adsorbate (up to some maximum binding energy) [32]; a certain degree of compliance with the Temkin model postulates was however implied owing to the values (>0.95) obtained for correlation coefficient R^2 . Additionally, the evaluated values of b_T were found to be much low. Since the values of b_T are approximate estimates of the heat of adsorption, such low values of b_T indicated low bonding energy between phenol and CTS activated carbon, clearly hinting at the weak interaction existing between the adsorbate and adsorbent [36], thus corroborating the suggestion of weak π – π dispersion interactions made earlier during the study of the adsorption process and during FTIR study.

3.5.4. Dubinin–Radushkevich isotherm

The Dubinin–Radushkevich isotherm model is an empirical model that quantifies, in particular, the adsorption mechanism which is characterized by a Gaussian energy distribution onto a heterogeneous surface; the applicability of this model in the present study was examined in order to explore the degree of irreversibility of the equilibrium adsorption process

under scrutiny [32]. The model is suitable for analysis of isotherms having high degree of rectangularity, high solute activities and fits the data in intermediate range of concentrations relatively well. The Dubinin–Radushkevich isotherm equation can be written as [37]:

$$q_e = q_s \exp(-B\varepsilon^2) \quad (10)$$

where q_s is the Dubinin–Radushkevich monolayer capacity (mg/g), B is isotherm constant related to sorption energy and ε is the Polanyi potential which is correlated to the equilibrium solution concentration of the adsorbate C_e (mg/L) as:

$$\varepsilon = RT \ln \left[1 + \frac{1}{C_e} \right] \quad (11)$$

where R is the gas constant (8.314 J/mol K) and T is the absolute temperature.

The isotherm constant B is related to mean free energy, E of adsorption per molecule of the adsorbate for transferring a molecule from its location in the sorption space, that is the solid surface to infinity in the solution and can be computed using the relationship [29]:

$$E = \frac{1}{\sqrt{2B}} \quad (12)$$

One of the unique features of the Dubinin–Radushkevich isotherm model observed by Foo and Hameed [32] is the fact that it is temperature dependent. The plot of $\ln(q_e)$ vs. ε^2 as shown in Fig. 5(d) enabled the determination of parameters q_s and E . Table 4 lists the parameters and the correlation coefficient R^2 for Dubinin–Radushkevich isotherm model.

The low values of R^2 indicated that the equilibrium relationship for adsorption of phenol onto CTS activated carbon could not be well emulated using Dubinin–Radushkevich isotherm model.

3.5.5. Type of adsorption isotherm

The adsorption isotherms for the adsorption of phenol onto CTS at 35°C (308 K) and 37°C (310 K) were found to be Type I isotherms, as indicated in Fig. 5(e). The theory behind Type I isotherms suggests that the potential field of force in action from the neighbouring walls of the very fine micropores present on the solid adsorbent surface, with dimensions of only about a few molecular diameters, would

overlap. This would lead an escalation in the interaction energy between the solid surface and the adsorbate molecules, resulting in an enhancement in the adsorption uptake, especially at lower equilibrium solution concentrations [18]. The interaction energy was considered to be large enough to bring about complete filling of the pores, which appeared as a plateau in Type I isotherm, thus indicating that at higher equilibrium solution concentrations the adsorption uptake was small; this suitably explained the levelling off of the curves. Type I isotherms hence ascertained the presence of micropores, reported earlier during the analysis of SE images (Fig. 1), with the help of the observation that the Type I isotherm plots; these plots did not exhibit a continuous monotonous rise but levelled off to a limiting value due to the narrow pores which could not accommodate more than a single molecular layer. This observation conformed to the suggestion of monolayer coverage made by Langmuir model, which usually provides the best explanation for the shape of the Type 1 adsorption isotherm. Also, the Type 1 adsorption isotherm plots in Fig. 5(e) indicated that at any particular equilibrium solution concentration, the quantum of phenol adsorbed at equilibrium demonstrated a significant escalation, following a slight decrease in process temperature from 310 to 308 K. This observation further substantiated the aforementioned conclusions drawn from careful analyses of the Langmuir and Temkin isotherm models, which had stipulated that the decrease in adsorption uptake following the increase in temperature had been primarily brought about by the relative dampening of the weak π - π dispersion interactions between the adsorbate molecules and the adsorbent [18,33,36]. This behaviour can additionally be attributed to the fact that exothermic adsorption processes such as the case investigated in the present study are often marked by the relatively enhanced propensity of the adsorbed solute molecules to escape into the bulk phase following the rise in temperature. In the present study, this tendency of the solute molecules was more pronounced at higher equilibrium solution concentrations and was considerably exacerbated in all likelihood by the low bonding energy between the adsorbate and the adsorbent as well as the probable distortions of some of the binding sites at the surface of the adsorbent. These factors thus explain the marked differences observed in the results obtained from the equilibrium studies that were conducted separately at different, albeit proximate experimental temperature values, namely 308 and 310 K, wherein the distinctions between the respective observations were relatively more conspicuous at higher equilibrium solution concentrations as highlighted in the

Type I isotherm plots (Fig. 5(e)) [38,39]. Herein, the minor aberrations from the expected trajectories could be attributed to experimental flaws, which were taken explicitly into account by way of errors bars, as exhibited in Fig. 5(e).

3.6. Adsorption kinetics

The transport of the adsorbates from the bulk solution to the surface of the porous adsorbents takes place by means of bulk solution transport, external (film) transport, internal (pore) transport and adsorption [26,29]. The transport steps occur in series, and the slowest step, called the rate-limiting step, controls the rate of removal. Recognition of adsorption kinetics enables the determination of the phenomenological coefficients which characterize the transport of adsorbate within adsorbents. Study of the kinetics of the adsorption process under scrutiny, was carried out using pseudo-first-order and pseudo-second-order kinetic models. Additionally, the intraparticle diffusion model was examined to identify and elucidate the diffusion mechanism while the Boyd kinetic model was analysed to predict the slowest step/steps constituting the adsorption process.

3.6.1. Pseudo-first-order kinetic model

Lagergren's pseudo-first-order kinetic model is in the form [26]:

$$\frac{dq}{dt} = k_1(q_e - q_t) \quad (13)$$

where q_e and q_t correspond to the amount of phenol adsorbed (mg/g) at equilibrium and at any time, t (min), respectively, and k_1 is the equilibrium rate constant of pseudo-first-order sorption (1/min). Integration of the above equation using the boundary conditions $t = 0 \rightarrow t$ and $q_t = 0 \rightarrow q_t$ results in the following equation in the linear form:

$$\log(q_e - q_t) = \log q_e - \frac{k_1}{2.303}t \quad (14)$$

The first-order rate constant k_1 was determined from the slope and intercept of plot of $\log(q_e - q_t)$ vs. t (Fig. 6(a)). The plot reflected that, the first-order equation of Lagergren did not suitably represent the kinetics of adsorption of phenol onto CTS activated carbon within the entire selected range of contact time; however a certain degree of compliance to the

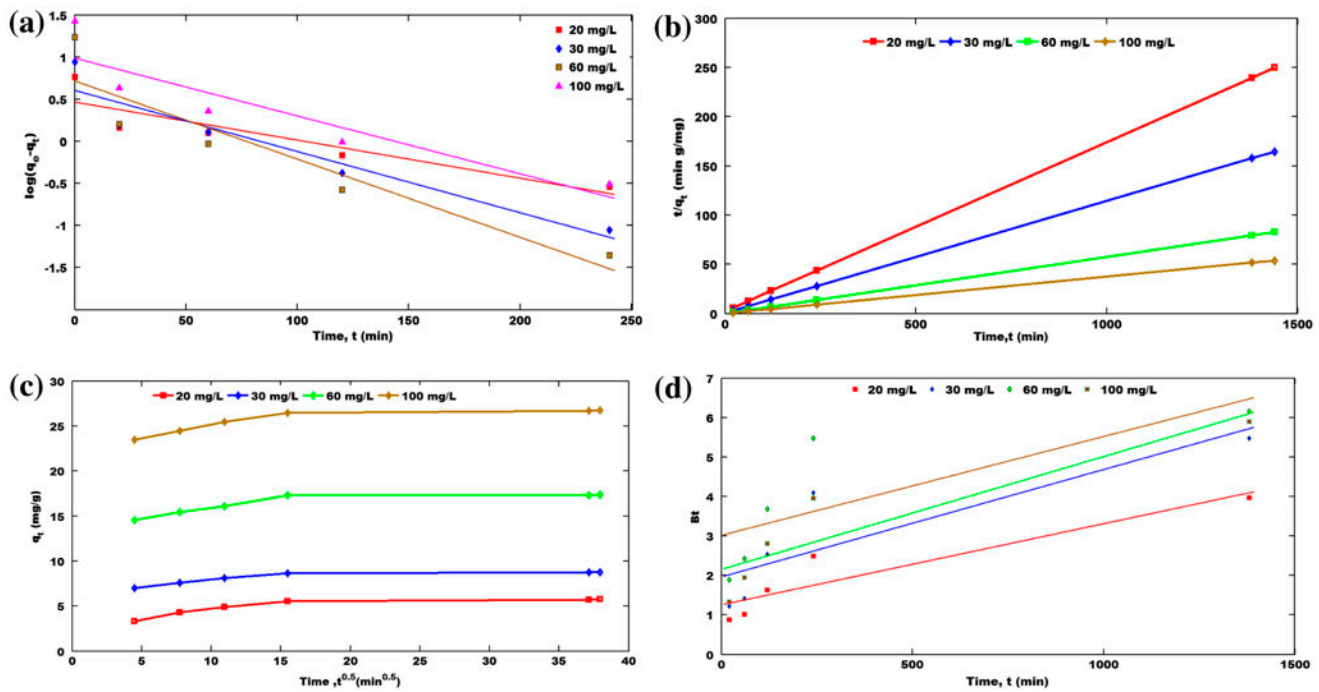


Fig. 6. (a) Pseudo-first-order-kinetics model for the adsorption of phenol onto CTS at 35°C (308 K) (the data points corresponding to 1,380 min were way too dispersed and hence were excluded from the plot). (b) Pseudo-second-order-kinetics model for the adsorption of phenol onto CTS at 35°C (308 K). (c) The intraparticle diffusion model for the adsorption of phenol onto CTS at 35°C (308 K). (d) The Boyd kinetic model for the adsorption of phenol onto CTS at 35°C (308 K).

pseudo-first-order kinetic model was observed generally over the initial stage of the adsorption process [29].

3.6.2. Pseudo-second-order model

Ho's pseudo-second-order model, which is based on equilibrium adsorption capacity of the solid phase, can be expressed as [29]:

$$\frac{dq}{dt} = k_2(q_e - q_t)^2 \quad (15)$$

where k_2 is the equilibrium rate constant of pseudo-second-order adsorption (g/mg min). Integrating the above differential equation using boundary condition $t = 0-t$ and $q_t = 0-q_t$, gives the following equation:

$$\frac{1}{(q_e - q_t)} = \frac{1}{q_e} + k_2 t \quad (16)$$

which can be rearranged as follows:

$$\frac{t}{q_t} = \frac{t}{q_e} + \frac{1}{k_2 q_e^2} \quad (17)$$

The plot of t/q_t vs. t is shown in (Fig. 6(b)). The equilibrium rate constant k_2 was calculated from the slope and intercept. The values of the correlation coefficient revealed that the adsorption mechanism reasonably obeyed pseudo-second-order model over the entire range of contact time, contrary to the observations obtained for pseudo-first-order model. Additionally, the initial adsorption rate h_0 (mg/g/min) pertaining to pseudo-second-order model at time $t = 0$ is defined as follows [26,40]:

$$h_0 = k_2 q_e^2 \quad (18)$$

The parameters of pseudo-first-order and pseudo-second-order models, along with their respective correlation coefficients, theoretical and experimental q_e values are listed in Table 5.

The comparison made between the values of the kinetic parameters and correlation coefficients of the pseudo-first-order model and those obtained for pseudo-second-order model in Table 5 clearly revealed that the correlation coefficient obtained for each phenol concentration by applying pseudo-second-order equation was relative higher than those obtained from pseudo-first-order equation; besides, the theoretical q_e

Table 5

The pseudo-first-order and pseudo-second-order kinetic parameters for the adsorption of phenol onto CTS at 35°C (308 K)

C_0 (mg/L)	q_e (exp) (mg/g)	Pseudo-first-order model			Pseudo-second-order model			
		k_1 (1/min)	q_e (cal) (mg/g)	R^2	k_2 (g/mg min)	q_e (cal) mg/g)	h_0 (mg/g/min)	R^2
20	5.8	0.013818	2.910717	0.831	0.012561	5.847953	0.429553	0.999
30	8.755556	0.020727	4.008667	0.904	0.017834	8.849558	1.396648	1.000
60	17.37778	0.016121	5.176068	0.871	0.026415	17.54386	8.130081	1.000
100	26.75556	0.009212	9.682779	0.838	0.008101	27.02703	5.91716	1.000

values evaluated from pseudo-second-order kinetic model conformed more precisely to the experimentally obtained q_e values as compared to q_e values obtained from pseudo-first-order model. Moreover, the increasing trend observed in the evaluated values of initial adsorption rate (h_0) and rate constant (k_2) of the pseudo-second-order model with the corresponding increase in the initial phenol concentration from 20 to 100 mg/L, highlighted the fact that enhancement in driving force for external mass transfer governed the adsorption process under scrutiny, thereby inducing substantial escalation in the equilibrium amount of phenol adsorbed; the concurrent antagonistic effect on the levels of the parameters h_0 and k_2 , brought about by the increased competition among the solute phenol molecules for the active sites on the activated carbon, was hence subdued [26,40]. It could thus be concluded that the pseudo-second-order kinetic model most appropriately defined the kinetics of adsorption of phenol on the CTS activated carbon. It further indicated that the adsorption process was governed by chemical sorption; this was partly due to the hydrogen bonding between the hydroxyl groups of phenol and the active functional groups in the adsorbent, and/or more importantly due to the π - π dispersion interaction between the adsorbate aromatic ring and the aromatic traits of the graphite structure, that is, due to any kind of valence force involved in sharing or exchange of electrons between the adsorbate and the functional groups present on the adsorbent surface. However, the slight decline in the value of rate constant k_2 corresponding to the increase in the initial phenol concentration to 100 mg/L hinted at the recognizable impact of the boundary layer resistance on the adsorption process when phenol solution of very high concentration (100 mg/L) was contacted with relatively insufficient amount (3 g/L) of CTS activated carbon; lack of available active sites at high concentration might have induced competition among the phenol molecules for the available adsorption sites on the activated carbon. These factors, consequently, resulted in prolongation

of the time of attainment of equilibrium adsorption capacity [28,40].

3.6.3 Intraparticle diffusion model

The diffusion mechanism was further explored using intraparticle diffusion model defined by Weber and Morris [26] as:

$$q_t = k_{pi}t^{1/2} + C_i \quad (19)$$

where k_{pi} (mg/g min^{1/2}), the intraparticle diffusion constant of stage i , was obtained from the slope of the straight line of q_t vs. $t^{1/2}$ (Fig. 6(c)), q_t is the amount of adsorbate adsorbed per unit mass of the adsorbent (mg/g) at any time t , C_i , the intercept of stage i , corresponds to the thickness of boundary layer, i.e. the larger the intercept, the greater the boundary layer resistance [11]. The plot of q_t vs. $t^{1/2}$ will be linear if the adsorption mechanism follows intraparticle diffusion and if the plot passes through the origin, then the rate-limiting step is only because of intraparticle diffusion. Otherwise, some other mechanism besides intraparticle diffusion is also involved in the adsorption process. The intraparticle diffusion model thus exhibits an empirical relationship, commonly applied to the most adsorption processes, where variation in uptake is almost proportional to $t^{1/2}$ rather than with the contact time t . The intraparticle diffusion plots (Fig. 6(c)), presenting the variation of q_t with $t^{1/2}$ for different initial concentrations, were multilinear. The multiple linearity in the plot indicated that more than one mechanism affected the phenol adsorption onto CTS [35]. Hameed et al. [29] observed similar trend in intraparticle diffusion plot for removal of phenol using rattan sawdust. The initial sharp section was attributed to rapid external surface adsorption and boundary layer diffusion of adsorbate, assuming convective mass transport [35]. The second stage represented the gradual adsorption stage, where

intraparticle diffusion was the rate-controlling step [26,35]. The last section, which usually corresponds to the final equilibrium stage occurring at higher concentrations, where the intraparticle diffusion would start to slow down owing to the extremely low adsorbate concentrations left in the aqueous solution, was absent in the present investigation [11,26]. The different stages in the rate of adsorption indicated that initially adsorption rate was faster and this rate of adsorptive uptake declined with time [11]. The values of k_{pi} , C_i and correlation coefficient R^2 obtained from the plots are listed in Table 6.

Fig. 6(c) also revealed that none of the lines passed through the origin. The deviation from origin or near saturation had probably taken place due to the difference in the rate of mass transfer between the initial and final stages of adsorption. This observation hence suggested that intraparticle diffusion was not the only rate-controlling step; the adsorption process was also governed by other mass transport mechanisms like boundary layer resistance, thus conforming to the conclusions drawn earlier from the analysis of pseudo-second-order kinetic model. Table 6 shows that with the enhancement in the initial concentration of the adsorbate solution a concomitant rise in the values of C_i was witnessed, which in turn indicated a dramatic escalation in the boundary layer thickness/resistance that could bring about a decrease in the external mass transfer rate and a simultaneous increase in internal mass transfer within the pores [26,41]. The value of k_{p1} corresponds to diffusion through macropores while k_{p2} relates to diffusion in meso and micropores [40,41]. The values of k_{p1} and k_{p2} exhibited in Table 6 also ascertained the fact that the intraparticle diffusional resistance in micro and mesopores was higher than that offered the macropores due to the reduction in the relative free path available for diffusion with corresponding decrease in pore width [40]. Furthermore, the increase in the rate parameter k_{p1} with corresponding enhancement in the initial concentration of the adsorbate, despite the accompanying increase in the boundary layer resistance (as indicated by C_i values), highlighted the fact that the external surface

adsorption or boundary layer diffusion was governed mostly by the initial concentration of the adsorbate solution and the driving force for external mass transfer associated with it; this observation thus substantiated the affirmations made by pseudo-second-order kinetic model which stated that the adsorption process was considerably influenced by the initial concentration of the phenol solution [41]; the effect of boundary layer resistance was found to be negligible at this stage. However, during the second stage dealing with gradual adsorption and intraparticle diffusion, the effect of escalation in boundary layer resistance on the diffusion through meso and micropores was notable, especially at the point where it succeeded in bringing about a decline in the corresponding value of rate parameter k_{p2} . The mutually opposing factors, namely enhancement in driving force due to increase in initial adsorbate concentration and associated rise in boundary layer resistance, moreover, resulted in an increment in the value of k_{p2} corresponding to initial phenol concentration of 100 mg/L, which was quite high, as compared to other phenol concentrations under study.

3.6.4. Boyd plot

The film resistance was further investigated by employing the Boyd film diffusion model [42]. The model, which assumes that the main resistance to diffusion is provided by the boundary layer surrounding the adsorbent particle, segregates the entire adsorption process into three sequential mechanistic steps, namely (i) film diffusion, involving transport of adsorbate ions towards the external surface of the adsorbent, (ii) particle diffusion, dealing with the migration and movement of adsorbate ions within the pores of the adsorbent; however, a small amount of adsorption occurring on the exterior surface of the adsorbent is neglected and finally the (iii) adsorption of the adsorbate ions onto the active sites present at the inside surface of the adsorbent. Furthermore, the third step is assumed to take place very fast and hence, is not considered as a potential rate-limiting

Table 6
Intraparticle diffusion constants for different initial phenol concentrations

C_0 (mg/L)	0–120 min			120–1,440 min		
	k_{p1} (mg/g min ^{0.5})	C_1	R^2	k_{p2} (mg/g min ^{0.5})	C_2	R^2
20	0.112	3.781	0.969	0.011	5.329	0.964
30	0.143	6.532	0.936	0.003	8.611	0.956
60	0.143	15.28	0.919	0.001	17.30	0.776
100	0.356	21.33	0.913	0.013	26.24	0.989

step by the Boyd kinetic model [26]. The Boyd kinetic model can be expressed as follows [40]:

$$F(t) = 1 - \left(\frac{6}{\pi^2}\right) \sum_{n=1}^{\infty} \left(\frac{1}{n^2}\right) \exp(-n^2Bt) \quad (20)$$

where $F(t)$ represents the fractional attainment of equilibrium at any time t and B (min^{-1}) is the Boyd's constant. Bt is mathematical function of $F(t)$.

$$F(t) = \frac{q_t}{q_e} \quad (21)$$

where q_e (mg/g) is the amount of adsorbate adsorbed at equilibrium per unit mass of adsorbent and q_t (mg/g) is the amount of adsorbate adsorbed per unit mass of adsorbent at any time t (minutes).

On application of the Fourier transform, the simplified representations of Bt obtained as mathematical function of $F(t)$ are listed below [40]:

$$\text{For } F(t) > 0.85, \quad Bt = 0.4977 - \ln(1 - F(t)) \quad (22)$$

$$\text{while, for } F(t) < 0.85, \quad Bt = \left(\sqrt{\pi} - \sqrt{\pi - \left(\frac{\pi^2 F(t)}{3}\right)^2}\right)^2 \quad (23)$$

The plot of calculated Bt values against time t is shown in Fig. 6(d).

The figure revealed that neither of the lines obtained for various initial phenol concentrations in solution passed through the origin and the measured points for each linear plot were scattered, that is the values of the correlation coefficient R^2 were quite low, as can be visualized in Table 7.

This indicated that the adsorption of phenol on the adsorbent was mainly governed by external mass transport mechanism with the film diffusion and chemical sorption (according to pseudo-second-order kinetic model) as the rate-limiting steps [41].

Table 7
Boyd plot parameters for different initial phenol concentrations

C_0 (mg/L)	Intercept	R^2
20	1.252	0.860
30	1.960	0.740
60	3.014	0.596
100	2.150	0.824

Meticulous analyses of the Boyd film diffusion model, intraparticle diffusion model and the pseudo-second-order kinetic model thus provided a comprehensive mechanistic understanding of the adsorption process, and more importantly corroborated the earlier statements, which had attributed the temporal protraction of the adsorption process to its relatively lengthy mass transport steps, namely film diffusion and chemical sorption, which, in accordance with the aforementioned kinetic models, were the rate-limiting steps of the adsorption process examined in the present study [29].

4. Desorption studies

The regeneration efficiency of spent adsorbent depends on the electron-donating property of adsorbed molecule; desorption of previously adsorbed phenol molecules from the adsorbent surface is rendered difficult owing to the strong electron-donating ability of the phenol molecules as reported in the literature [9,13]. Desorption studies were, hence, carried out in order to examine the regeneration potential of spent activated carbon loaded with phenol.

While no amount of phenol was desorbed using water, sodium hydroxide solution was able to recover about 53%. Absolute ethanol demonstrated desorption efficiency as high as 96%, thus emerging as the best and the most promising desorbing agent among the three. Earlier, Tan et al. [11] had made similar observations, reporting a regeneration efficiency of 99.6% for 2,4,6-trichlorophenol desorption from oil palm empty fruit bunch-based activated carbon using ethanol which was much high compared to that achieved using NaOH desorption method.

Desorption of phenol using 0.1 (N) NaOH can be elucidated further with the help of similar explanation used earlier to justify the effect of pH on the adsorption process, which had illustrated the fact that basic pH values >7 , that is at $\text{pH} > \text{p}K_a$ ($\text{p}K_a$ for phenol ≈ 9.89) associated with sodium hydroxide 0.1 (N), the phenols dissociated to give phenolate ($\text{C}_6\text{H}_5\text{O}^-$) ions. These ions were negatively charged. At such high basic pH values, the functional groups (acidic) at the surface of the adsorbent ionized, in most cases, partially, to give the surface of the adsorbent a negative charge. As a result, electrostatic repulsive interactions took place between the CTS surface and the phenolate ions [18,19]. The electrostatic repulsion between the negative surface charge and the phenolate anions could be responsible for the satisfactory elution of phenol obtained using sodium hydroxide solution. Moreover, the reaction between NaOH and phenol, resulting in the formation of a phenol-sodium salt facilitated desorption of phenol from the CTS surfaces.

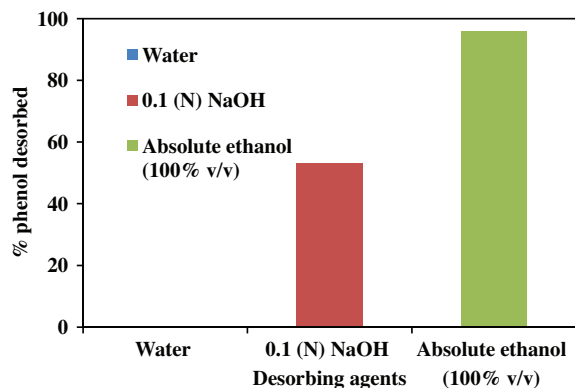


Fig. 7. Fraction of desorbed phenol from CTS activated carbon by different desorbing solutions (adsorbent dose: 0.1 g; time: 24 h; temperature: 36°C 309 K).

Desorption of the adsorbed phenol using ethanol, however, occurred owing to the fact that ethanol, being probably a much better solvent for phenol than solvent water, succeeded to a great extent in weakening the adsorptive interaction between phenol and the surface of the CTS adsorbent [13], as is evident from the reasonably high recorded results, contrary to the ones obtained from other reported investigations [9]. The performance of the various desorbing agents under scrutiny in the present investigation can be visualized in Fig. 7.

The efficiency of spent CTS activated carbon regenerated chemically using absolute ethanol (100% v/v) can be visualized in Table 8.

The CTS activated carbon regenerated using ethanol was found to retain 95% of its original adsorption efficiency after a single cycle of operation comprising adsorption and desorption, which was quite satisfactory.

4.1. Application of thermogravimetric analysis (TGA) to CTS activated carbons for determination of its thermal stability and feasibility of the method used in regenerating activated carbon loaded with phenol using absolute ethanol

Activated carbons suffer from some serious handicaps like high regeneration losses and continuous

decrease in sorption capacity with each regeneration cycle when they are subjected to conventional thermal regeneration method that involves reactivation in oxidizing atmosphere at elevated temperatures, where high amounts of carbon are consumed. The present investigation was carried out with an objective to deduce a suitable method for improving the regeneration yield of CTS activated carbon contaminated with phenol, with the aid of thermogravimetric (TGA) analysis. The analysis of the TGA curves provided an insight into the thermal stability of the CTS activated carbon and the difference in thermal stabilities of the chemisorbed oxygen constituting different surface oxygen groups thereof, involving different sites with varying energies; hence the nature of adsorption that had occurred in the present study was also evaluated; besides, the efficiency of recovery of adsorbed phenol from the occupied active sites of CTS activated carbon surface using organic absolute ethanol (100% v/v) solvent was also examined, where absolute ethanol was selected owing to its spectacular performance as the most promising desorbing agent. Fig. 8(a) exhibits the TGA plot for CTS activated carbon in terms of weight (%) vs. temperature. The initial loss in weight of the CTS activated carbon sample at lower temperatures below 200°C as revealed in TGA curve of Fig. 8(a) indicated elimination of moisture [18]. The sample remains approximately stable in the temperature range of 200–600°C and a very gradual decrease in weight (%) was attributed to decomposition of lignocellulosic biomass comprising cellulose, hemicellulose and lignin, with evolution of volatile matter obtained from primary carbonization [43]. A prominent decrease in the weight (%) of the sample is witnessed beyond 596°C right up to 850°C; this weight loss corresponded partly to evolved hydrogen atoms desorbed as a result of splitting of C-H bonds in the temperature range 500–1,000°C, and mainly to the evolution of CO by the decomposition of aromatic rings which, according to the FTIR analysis, were present on the activated carbon surface [18].

Fig. 8(b) presents the TGA plot for phenol-loaded CTS activated carbon expressed as weight (%) vs.

Table 8

Variation in efficiency of CTS activated carbon after a cycle of operation involving phenol adsorption followed by regeneration of spent activated carbon using ethanol

Adsorbent dosage (g/L)	Initial phenol concentration (mg/L)	Phenol uptake, C_{ad} (mg/g)	Phenol uptake, C_{ad1} by spent CTS activated carbon regenerated using ethanol (mg/g)	Fraction of original adsorption efficiency retained, $\frac{C_{ad1}}{C_{ad}} \times 100$ (%)
1.0	2,000	36.67	–	95
1.0	2,000	–	34.8	

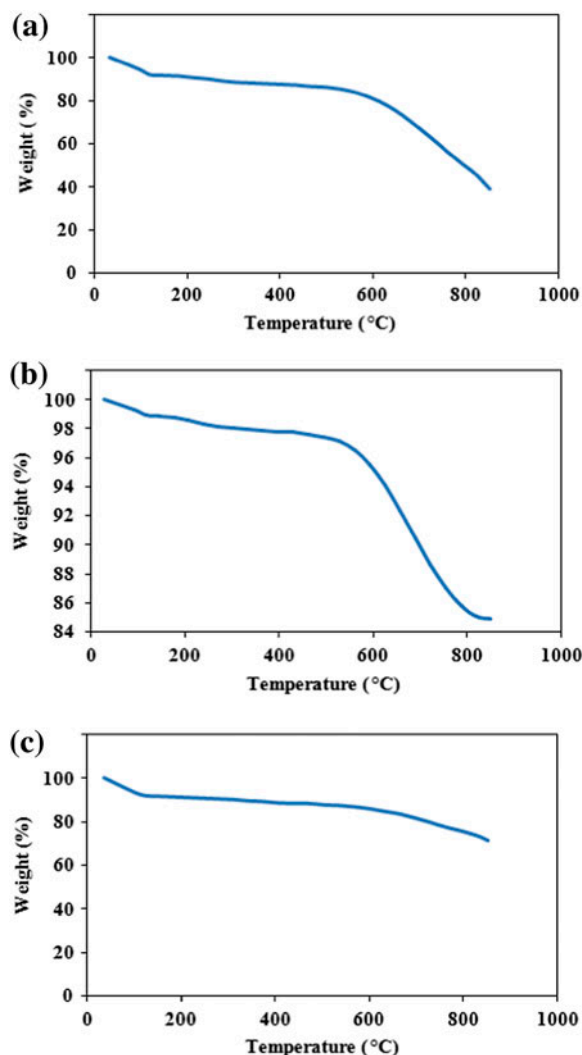


Fig. 8. TGA curves in terms of weight (%) of the sample vs. temperature (°C) for (a) CTS activated carbon; (b) phenol loaded CTS activated carbon; (c) spent activated carbon treated with ethanol.

temperature, where the initial loss in weight below 115°C was attributed to the loss of traces of moisture remaining in the sample even after drying the sample of spent activated carbon at 110 °C in an air oven. The TGA curve in the figure revealed two shoulders, similar to the observations made by other scientists [16]. Appearance of the first peak in the range 115.87–494.94°C, centred at 200°C, marked the commencement of desorption of phenol physisorbed onto the active sites on the activated carbon surface, owing to the fact that the normal boiling point of phenol is 181.75°C [44]. The second relatively prominent peak was visualized in the temperature range 494.94–600°C and it indicated the beginning of the desorption of phenol bound to active sites on CTS activated carbon mostly

by chemisorption [16,44], which continued up to 850°C temperature. The escalation in residual weight (%) obtained for spent CTS activated carbon (85% as shown in Fig. 8(b)) as compared to weight residue (%) obtained for original activated carbon sample (40% as shown in Fig. 8(a)) at the end of programmed thermodesorption can be reasonably explained by the fact that most of the chemically sorbed phenol molecules had probably undergone decomposition on the surface causing the diminution or closing of some pores with carbon atoms or char obtained as products of decomposition or active pyrolysis, which had additionally contributed to the enhancement in the residual weight of the phenol-loaded CTS activated carbon [16,19].

Finally, the performance efficiency of organic absolute ethanol (100% v/v) solvent as a desorbing agent was examined using the TGA plot obtained for spent activated carbon treated with ethanol and presented in Fig. 8(c). As shown in Fig. 8(c), an initial significant decrease in weight (%) was denoted by a sharp drop in the TGA curve near 122°C, probably due to loss of traces of adsorbed ethanol remaining on the surface of the activated carbon even after drying the sample at 110°C (383 K) in the air oven. Ethanol, being a better solvent for phenol than water, was capable of weakening the adsorptive interaction between phenol and adsorbent surface, which resulted in relative smooth and unperturbed TGA curve and disappearance of peaks earlier visualized in the TGA plot for spent CTS activated carbon (Fig. 8(b)); however, the slight decline in sample weight observed in the temperature range 400–800°C was attributed to the thermal desorption of chemisorbed phenol molecules, which could not be removed using ethanol [16,44].

5. Conclusion

The present investigation clearly established CTS activated carbon as a viable low-cost alternative of commercial activated carbon for application in phenol removal from the effluent discharged by various industries; besides, valorizing agricultural residues to prepare activated carbon, could also successfully address the problem of disposal of agricultural wastes. Additionally, adopting CTS activated carbon as potential adsorbents in various industries could also result in economizing the cost of adsorbent production, and hence entire effluent treatment process could be reduced, due to easy availability of raw materials. The excellent maximum adsorption capacity of 41.6667 mg/g, the enhanced BET surface area and pore volume, high carbon content, low ash content and other physicochemical properties analysed using different characterization procedures further

ascertained the comparability of the prepared adsorbent with commercial activated carbon in terms of quality. The competence of CTS activated carbon adsorbent in the field of environmental pollution abatement was thereby certified. The spectacular regeneration and recycling potential of the activated carbon, as revealed in the desorption studies, was further corroborated by means of TGA plots; the results indicated that the activated carbon prepared was successful, albeit to a certain extent, in overcoming the serious handicaps like regeneration loss, high cost, etc., that commercial activated carbons usually suffer from. In this context, it can as well be suggested that the regeneration potential of the prepared CTS activated carbons can be further improved by minimizing the possibility of chemisorption of phenol on to the carbon surface, which can otherwise render the regeneration of spent activated carbon difficult; this can be done by implementing certain measures such as, mild oxidation of activated carbon using oxygen, selecting a lower temperature for phenol adsorption and reduction in the duration between the first contact of activated carbon with phenol and its subsequent regeneration.

Acknowledgement

The authors would like to express their sincerest gratitude to Prof (Dr) Tarkeshwar Kumar, Director, National Institute of Technology, Durgapur for providing the necessary laboratory facilities and to National Metallurgical Laboratory (NML), Jamshedpur for providing the EPMA equipment to analyse samples. The authors are also thankful to the faculty members at Gupta College of Technological Sciences, Asansol, for supporting the research through their assistance in carrying out FTIR analysis of samples in their laboratory.

Nomenclature

Symbols

q_e (mg/g)	— equilibrium amount of adsorbate (phenol) adsorbed per unit mass of adsorbent, (mg of adsorbate/g of adsorbent)
C_0 and C_e (mg/L)	— initial and equilibrium liquid-phase concentrations of phenol, respectively
V (L)	— volume of the adsorbate solution
m (g)	— the mass of dry adsorbent used
C_{ad} (mg/g of adsorbent)	— phenol uptake per unit weight of adsorbent

C_{de} (mg/g of adsorbent)	— phenol desorbed from unit weight of spent adsorbent
φ_{ions}	— ionic fraction of phenolate ion
T (K)	— temperature of adsorption
b (L/mg)	— Langmuir isotherm constant
q_{max} (mg/g)	— Langmuir isotherm constant representing the surface concentration at monolayer coverage
R_L	— separation factor
R^2	— correlation coefficient
R	— universal gas constant (8.314 J/mol K)
K_F ((mg/g) (L/mg) ^{1/n})	— Freundlich isotherm constant related to adsorption capacity
$(1/n)$ (unitless)	— Freundlich isotherm constant related to adsorption intensity.
A (L/g)	— Temkin isotherm equilibrium binding constant
b_T (J/mol)	— reciprocal of adsorption capacity of the adsorbent
B	— Temkin isotherm constant
B (mol ² /kJ ²)	— Dubinin–Radushkevich isotherm constant
ε	— Polanyi potential
E (kJ/mol)	— mean free energy
q_s (mg/g)	— Dubinin–Radushkevich monolayer capacity
q_t (mg/g)	— amount of adsorbate (phenol) adsorbed g of adsorbent at any time, t (min)
k_1 (min ⁻¹)	— equilibrium rate constant of pseudo-first-order sorption
k_2 (g/mg min)	— equilibrium rate constant of pseudo-second-order adsorption
h_0 (mg/g/min)	— initial adsorption rate
$q_e(cal)$ (mg/g)	— calculated adsorbate concentration at equilibrium
$q_e(exp)$ (mg/g)	— experimental adsorbate concentration at equilibrium
k_{pi} (mg/g min ^{1/2})	— the intraparticle diffusion constant of stage i
F	— Boyd constant represents the fraction of solute adsorbed at any time t
B (min ⁻¹)	— Boyd's constant
Bt	— a mathematical function of F in Boyd kinetic model

Abbreviations

RSM	— response surface methodology
CCD	— central composite design
CTS	— charred tomato stem
EPMA	— electron probe microanalysis
SEI	— secondary electron imaging
SEM	— scanning electron microscopy
EDS	— energy dispersive spectrometry
FTIR	— Fourier transform infrared
TGA	— thermogravimetric analysis

References

- [1] Agency for Toxic Substances and Disease Registry (ATSDR), Toxicological profile for phenols (Draft). US Public Health Service, US Department of Health & Human Services, Atlanta, GA, 1990.
- [2] World Health Organization (WHO), International standards for Drinking Water, Geneva, 1963, p. 40.
- [3] Z. Zeng, H. Zou, X. Li, M. Arowo, B. Sun, J. Chen, G. Chu, L. Shao, Degradation of phenol by ozone in the presence of Fenton reagent in a rotating packed bed, *Chem. Eng. J.* 229 (2013) 404–411.
- [4] M. Caetano, C. Valderrama, A. Farran, J.L. Cortina, Phenol removal from aqueous solution by adsorption and ion exchange mechanisms onto polymeric resins, *J. Colloid Interface Sci.* 338 (2009) 402–409.
- [5] O. Abdelwahab, N.K. Amin, E.-S.Z. El-Ashtouky, Electrochemical removal of phenol from oil refinery wastewater, *J. Hazard. Mater.* 163 (2009) 711–716.
- [6] H.-Q. Li, H.-J. Han, M.-A. Du, W. Wang, Removal of phenols, thiocyanate and ammonium from coal gasification wastewater using moving bed biofilm reactor, *Bioresour. Technol.* 102 (2011) 4667–4673.
- [7] A.T. Mohd Din, B.H. Hameed, A.L. Ahmad, Batch adsorption of phenol onto physiochemical-activated coconut shell, *J. Hazard. Mater.* 161 (2009) 1522–1529.
- [8] M. Ahmaruzzaman, Adsorption of phenolic compounds on low-cost adsorbents: A review, *Adv. Colloid Interface Sci.* 143 (2008) 48–67.
- [9] L.A. Rodrigues, M.L.C.P. da Silva, M.O. Alvarez-Mendes, A. Coutinho, G.P. Thim, Phenol removal from aqueous solution by activated carbon produced from avocado kernel seeds, *Chem. Eng. J.* 174 (2011) 49–57.
- [10] L.J. Kennedy, J.J. Vijaya, K. Kayalvizhi, G. Sekaran, Adsorption of phenol from aqueous solutions using mesoporous carbon prepared by two-stage process, *Chem. Eng. J.* 132 (2007) 279–287.
- [11] I.A.W. Tan, A.L. Ahmad, B.H. Hameed, Adsorption isotherms, kinetics, thermodynamics and desorption studies of 2,4,6-trichlorophenol on oil palm empty fruit bunch-based activated carbon, *J. Hazard. Mater.* 164 (2009) 473–482.
- [12] M. Zhong, Y. Wang, J. Yu, Y. Tian, G. Xu, Porous carbon from vinegar lees for phenol adsorption, *Particology* 10 (2012) 35–41.
- [13] L.A. Rodrigues, L.A. de Sousa Ribeiro, G.P. Thim, R.R. Ferreira, M.O. Alvarez-Mendez, A. dos Reis Coutinho, Activated carbon derived from macadamia nut shells: An effective adsorbent for phenol removal, *J. Porous Mater.* 20 (2013) 619–627.
- [14] National Horticulture Board, Indian Horticulture Database, Ministry of Agriculture, Government of India, Gurgaon, 2011.
- [15] S. Chatterjee, A. Kumar, S. Basu, S. Dutta, Application of response surface methodology for methylene blue dye removal from aqueous solution using low cost adsorbent, *Chem. Eng. J.* 181–182 (2012) 289–299.
- [16] P. Magne, P.L. Walker Jr, Phenol adsorption on activated carbons: Application to the regeneration of activated carbons polluted with phenol, *Carbon* 24 (1986) 101–107.
- [17] J.T. Nwabanne, P.K. Igbokwe, Application of response surface methodology for preparation of activated carbon from palmyra palm nut, *N Y Sci. J.* 5 (2012) 18–25.
- [18] R.C. Bansal, M. Goyal, Activated Carbon Adsorption, CRC Press, USA, 2005.
- [19] H. Marsh, F. Rodriguez-Reinoso, Activated Carbon, Elsevier Ltd., Oxford, U.K., 2006.
- [20] P. Girods, A. Dufour, V. Fierro, Y. Rogaume, C. ogaume, A. Zoulalian, A. Celzard, Activated carbons prepared from wood particleboard wastes: Characterisation and phenol adsorption capacities, *J. Hazard. Mater.* 166 (2009) 491–501.
- [21] M. Molina-Sabio, F. RodRíguez-Reinoso, F. Caturla, M.J. Sellés, Porosity in granular carbons activated with phosphoric acid, *Carbon* 33 (1995) 1105–1113.
- [22] S. Dutta, A. Bhattacharyya, A. Ganguly, S. Gupta, S. Basu, Application of response surface methodology for preparation of low-cost adsorbent from citrus fruit peel and for removal of methylene blue, *Desalination* 275 (2011) 26–36.
- [23] M. Al Bahri, L. Calvo, M.A. Gilarranz, J.J. Rodriguez, Activated carbon from grape seeds upon chemical activation with phosphoric acid: Application to the adsorption of diuron from water, *Chem. Eng. J.* 203 (2012) 348–356.
- [24] J. Coates, Interpretation of infrared spectra, a practical approach, in: R.A. Meyers (Ed.), *Encyclopedia of Analytical Chemistry*, John Wiley & Sons Ltd, Chichester, 2000, pp. 10815–10837.
- [25] R.M. Silverstein, G.C. Bassler, T.C. Morrill, *Spectrometric Identification of Organic Compounds*, fifth ed., John Wiley and Sons, New York, NY, 1991.
- [26] B.H. Hameed, I.A.W. Tan, A.L. Ahmad, Adsorption isotherm, kinetic modeling and mechanism of 2,4,6-trichlorophenol on coconut husk-based activated carbon, *Chem. Eng. J.* 144 (2008) 235–244.
- [27] R.W. Coughlin, F.S. Ezra, Role of surface acidity in the adsorption of organic pollutants on the surface of carbon, *Environ. Sci. Technol.* 2 (1968) 291–297.
- [28] B.K. Dutta, *Principles of Mass Transfer and Separation Processes*, PHI Learning Private Limited, New Delhi, 2009, pp. 609–650.
- [29] B.H. Hameed, A.A. Rahman, Removal of phenol from aqueous solutions by adsorption onto activated carbon prepared from biomass material, *J. Hazard. Mater.* 160 (2008) 576–581.
- [30] J.S. Mattson, H.B. Mark Jr, M.D. Malbin, W.J. Weber Jr, J.C. Crittenden, Surface chemistry of active carbon: Specific adsorption of phenols, *J. Colloid Interface Sci.* 31 (1969) 116–130.
- [31] R.S. Boethling, D. Mackay (Eds.), *Handbook of Property Estimation Methods for Chemicals: Environmental Health Sciences*, CRC Press, USA, 2000.
- [32] K.Y. Foo, B.H. Hameed, Insights into the modeling of adsorption isotherm systems, *Chem. Eng. J.* 156 (2010) 2–10.
- [33] S. Larous, A.H. Meniai, The use of sawdust as by product adsorbent of organic pollutant from wastewater: adsorption of phenol, *Energy Proc.* 18 (2012) 905–914.
- [34] O. Hamdaoui, E. Naffrechoux, Modeling of adsorption isotherms of phenol and chlorophenols onto granular activated carbon Part I. Two-parameter models and equations allowing determination of thermodynamic parameters, *J. Hazard. Mater.* 147 (2007) 381–394.

- [35] V.C. Srivastava, M.M. Swamy, I.D. Mall, B. Prasad, I.M. Mishra, Adsorptive removal of phenol by bagasse fly ash and activated carbon: equilibrium, kinetics and thermodynamics, *Colloids Surf., A* 272 (2006) 89–104.
- [36] V. Srihari, A. Das, Comparative studies on adsorptive removal of phenol by three agro-based carbons: Equilibrium and isotherm studies, *Ecotoxicol. Environ. Saf.* 71 (2008) 274–283.
- [37] P. Senthil Kumar, S. Ramalingam, C. Senthamarai, M. Niranjanaa, P. Vijayalakshmi, S. Sivanesan, Adsorption of dye from aqueous solution by cashew nut shell: Studies on equilibrium isotherm, kinetics and thermodynamics of interactions, *Desalination* 261 (2010) 52–60.
- [38] A.A. Lewinsky, *Hazardous Materials and Wastewater: Treatment, Removal and Analysis*, Nova Science Publishers, New York, NY, 2007.
- [39] S. Al-Asheh, Z. Duvnjak, Adsorption of copper and chromium by *Aspergillus carbonarius*, *Biotechnol. Prog.* 11 (1995) 638–642.
- [40] B.H. Hameed, M.I. El-Khaiary, Malachite green adsorption by rattan sawdust: Isotherm, kinetic and mechanism modeling, *J. Hazard. Mater.* 159 (2008) 574–579.
- [41] M.U. Dural, L. Cavas, S.K. Papageorgiou, F.K. Katsaros, Methylene blue adsorption on activated carbon prepared from *Posidonia oceanica* (L.) dead leaves: Kinetics and equilibrium studies, *Chem. Eng. J.* 168 (2011) 77–85.
- [42] G.E. Boyd, A.W. Adamson, L.S. Myers, The exchange adsorption of ions from aqueous solutions by organic zeolites. II. Kinetics 1, *J. Am. Chem. Soc.* 69 (1947) 2836–2848.
- [43] H. Hadoun, Z. Sadaoui, N. Souami, D. Sahel, I. Toumert, Characterization of mesoporous carbon prepared from date stems by H₃PO₄ chemical activation, *Appl. Surf. Sci.* 280 (2013) 1–7.
- [44] N. Tancredi, N. Medero, F. Möller, J. Píriz, C. Plada, T. Cordero, Phenol adsorption onto powdered and granular activated carbon, prepared from Eucalyptus wood, *J. Colloid Interface Sci.* 279 (2004) 357–363.